Studies of Radiative Cooling at Land Basins in Snowy Season*

by

Nobuyoshi ISHIKAWA
石 川 信 敬
The Institute of Low Temperature Science

Received November 1977

Abstract

Observations were carried out of temperature inversion due to radiative cooling at land basins in snowy seasons, which resulted in the obtaining of the meteorological conditions, which were necessary for inducing the phenomena of remarkable inversion and very low temperatures at the bottom of such basins. Heat balances were also observed in each basin by accurate measurements at two meteorological sites having an altitude difference of 250 m, the one being at the bottom of the basin and the other on top of a mountain surrounding it. It was found that the difference of heat balance components at both places was the main cause of the phenomena. Namely, a heat sink was due only to nocturnal radiation, and in case of small sensible and latent heat fluxes, which appeared when wind speed was very small, the extensive cooling took place at the lower parts of the basin. On the other hand, a large sensible heat flux was observed at the higher part of surrounding mountains because a comparatively strong wind blowed usually, as a result of which an air to snow heat transfer compensated for a heat loss due to radiation. Therefore, temperature variations at the higher parts of surrounding mountains became small in contrast with large temperature variations at the bottom of the basin, where temperature fell down to very low degrees. It gave rise to a strong inversion between the two different altitudes.

Cooling rates were predicted numerically in the lower part of atmosphere by solving a heat balance equation at the surface of the basin, whereby calculated values were in good agreement with observed data.

Finally, a measurement was made of the down air flow along a mountain slope, whereby its contribution to the cooling rates over the bottom was found less important.

* Contribution No. 1874 from the Institute of Low Temperature Science.
北海道大学審査学位論文

Contents

I. Introduction

Knowledge of climatic characteristics of a small area calls for different approaches such as observations of air flow patterns in the area and investigations of heat balance at the ground or snow surface. As for the former approach, the observation provides a relation between the distributions of meteorological elements and flow patterns. Namely, the climatic characteristics of the area is explained by local differences of air currents. Using this approach many investigations have been extensively conducted since the end of the nineteenth century (GEIGER 1965, YOSHINO 1971, 1975). They have been followed by the latter approach with the progress in development of sophisticated instruments. This approach has also been adopted by a number of investigators studying mass balances of glaciers (WENDLER and ISHIKAWA 1973, WENDLER and WELLER 1974, LaCHAPELLE 1959) or amount of snowmelt on a snow surface (de LaCASINIÈRE 1974, KOJIMA and others 1971), whereas it has been very rarely attempted to explain the climatic pattern of an area by means of the results of actual observations of areal heat balance variation in the area (WENDLER and ISHIKAWA 1973).

Radiative cooling constitutes a well-known microclimatic phenomenon at a land basin. It brings about a temperature inversion between two different altitudes, as a result of which it is likely that the air temperature at a mountaintop surrounding the basin is higher than that at the basin. From the approach of air flow patterns it has been believed that the cause of the phenomenon of the lowering temperatures at the basin is due to deposition of a cold air which has been created on surrounding mountain slopes (YOSHINO 1971).

Meanwhile, studies of this phenomenon by the heat balance approach and actual measurements of nocturnal radiation amount are very few (WENDLER 1971, WENDLER and JAYAWEERA 1972).

The present author has investigated the mechanism of radiative cooling at a land basin covered by a snow pack and tried to explain it from a heat balance viewpoint using the results obtained by this approach. The results are reported and discussed in this paper, which is composed of the following four parts :

1) Observations of processes and intensities of radiative cooling occurring in land basins under characteristic weather conditions for such cooling.
2) Studies of areal and seasonal variations of each component of a heat balance equation during radiative cooling on the basis of the meteorological elements observed.
3) Numerical calculations applied to time variations of air and snow temperature profiles and of heat balance at the snow surface; comparison of the computed with the observed results.
4) Discussions of causes of a temperature inversion at a land basin.

II. Observational sites and instrumentation

A snow cover behaves nearly as a black body concerning long-wave radiation (MUNN 1966). Meanwhile, the character of a land surface without a snow cover varies considerably from place to place, but, when it is covered with snow, its surface can be assumed nearly homogeneous, making it easy to obtain a heat balance at the surface. Therefore, the observations reported were made during snowy seasons from January 1971 to April 1976. Observational sites were set at the Teshio Experimental Forest in Toikanbetsu (Fig. 1.a) and the Uryu Experimental Forest in Moshiri (Fig. 1. b), both of Hokkaido University, which are located in the northern part of Hokkaido, where extremely low temperatures are observed frequently every winter. Each experimental forest is in a mountaineous region, surrounded by mountains with an altitudinal difference of about 250 m in height between the mountaintops and the bottom of the basin. Another observational site was set in hilly country at the Tomakomai Experimental Forest of the same university in the central part of Hokkaido, whose altitudinal difference between the higher and the lower part is about 40 m.

At each site two meteorological stations were set up, the one at the lower part of the basin and the other at the highest part of a surrounding mountain, while along a mountain slope air temperature and wind speed were measured using simple and handy instruments. Following are observational items and instruments at each site :

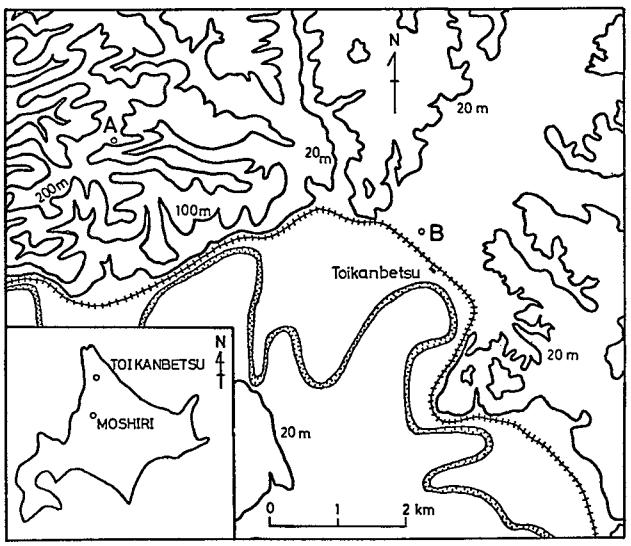

Fig. 1. (a) Location map of two meteorological stations in Toikanbetsu.
A: higher station B: lower station

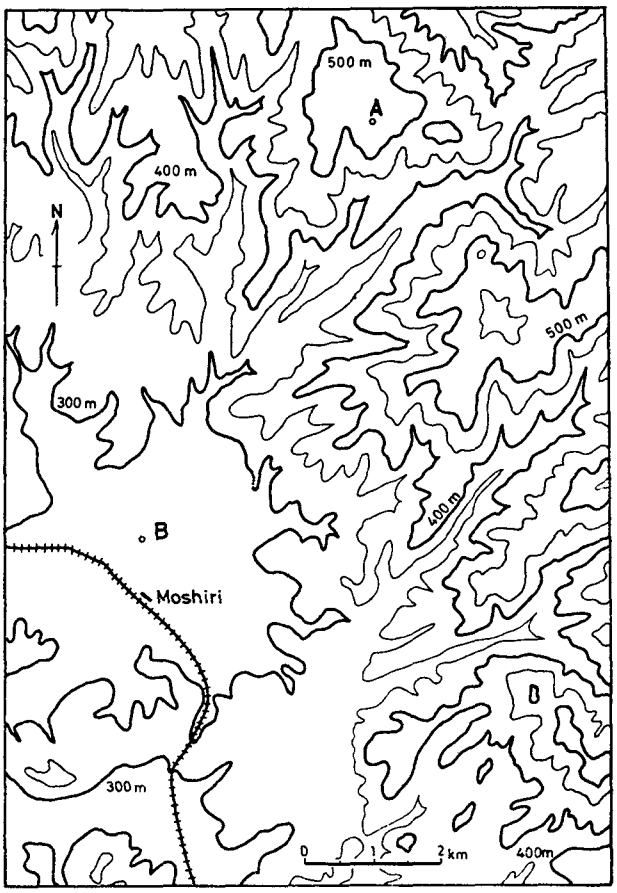

Fig. 1. (b) Location map of two heat balance stations in Moshiri.
A: higher station B: lower station

A) *At the lower station*

Air temperature (profile)	Ventilated resistance thermometers
Wind speed (profile)	An aerovane anemometer and three-cup anemometers
Humidity (profile)	Ventilated wet resistance thermometers and a hair-hygrometer
Amount of net radiation	Funk-type (CN-1, CN-2) net radiometers
Amounts of atmospheric radiation and terrestrial radiation	GARP-type MS-4R radiometers
Amounts of incoming and outgoing	Pyranometers

solar radiation	
Surface temperature	An infrared radiation thermometer and thermisters
Snow temperature (profile)	Thermister thermometers and thermocouples
Heat flux in a snow cover	TPD heat flow transducers
Free water content in a snow cover and amount of snowmelt	Yoshida's calorimeters and snow cover measurements
B) *At the higher station*	
Air temperature (profile)	Bimetal thermometers and ventilated resistance thermometers
Wind speed (profile)	Three-cup photo-electronic anemometers and Robinson anemometers
Humidity	Hair-hygrometers
Amount of radiation	Funk-type (CN-2) net radiometer
C) *At a mountain slope*	
Air temperature	Bimetal thermometers, and maximum and minimum thermometers
Wind speed	A three-cup Robinson anemometer
D) *At running measurements*	
Air temperature	Thermister thermometers
Wind speed	A thermister anemometer and Biramn anemometers

Data taken at running measurements were always corrected using the data taken at the lower station. All meteorological instruments were calibrated before and after each observation; in particular, the radiometers were calibrated and their data corrected by comparing them with the standard instruments of the Radiative Center of the Observation Division of the Japan Meteorological Agency.

III. Observational Results

III—1 *Meteorology during radiative cooling at a land basin*

(1) *Adiabatic and inversion conditions*

Figure 2 shows time variations of air temperature and amount of net radiation during a typical observational period, which were measured at the height of 25 and 120 cm above the snow surface, respectively. The higher station (A) is located at 235 m above sea level and the lower station (B) at 10 m. The data of air temperature taken at a 25 cm height above the surface at two other stations (one is at 35 m above mean sea

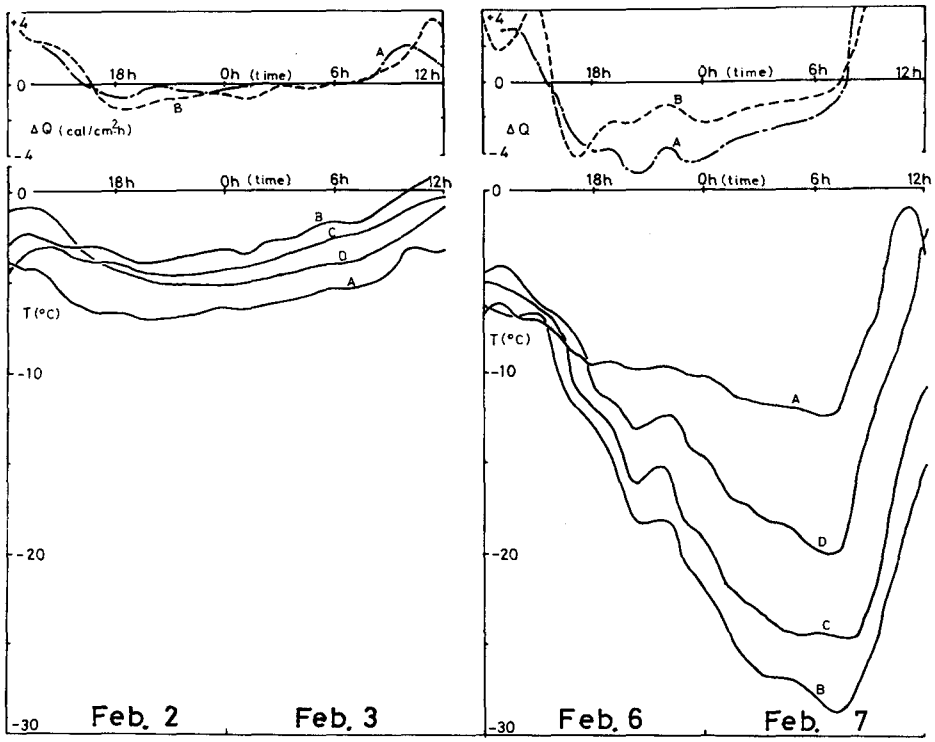

Fig. 2 Variations in mean hourly values of air temperature and net radiation flux at Toikanbetsu.

level (C) and the other at 135 m (D)) are also plotted in this figure. On Feb.2-3 the values of net radiation amount at two stations (A and B) were almost the same, nearly equal to zero. As to the air temperature, it took the highest value at the lower station, and gradually lowered with increasing altitude. On Feb.6-7 it was clearly shown that the extreme values of net radiation amount at two sites were found at around 1800 hours in the evening, and then gradually decreased during the night ; besides, the value of net radiation amount at the higher station (A) was larger than that at the lower station (B). Concerning the air temperature, the extremely low value was measured on the morning of Feb.7, but the air temperature at the upper station was higher than that at the lower station, which scarcely changed during the previous night. At the middle part of the mountain slope, it was found that the temperature decreased during the night, but it did not drop so much as it did at the lower station. From these observational results the condition in which the former took place may be called the adiabatic lapse condition, and the condition in which the latter took place the inversion condition. The inversion strength is assumed to be represented in this paper by the difference ΔT between the

temperature at the lower station T_B and the temperature at the higher station T_A, where the negative sign represents the temperature inversion.

(2) *Distributions of horizontal and vertical air temperatures at a land basin*

Air temperatures at a height of 1 m above the snow surface were observed at several points in a basin, whereby it was examined whether or not the values taken at the lower station represented the typical ones of the whole area of the basin. The horizontal temperature distributions immediately after sunset and immediately before sunrise in winter and the snow-melting season are shown respectively in Figs.3 and 4, in which the

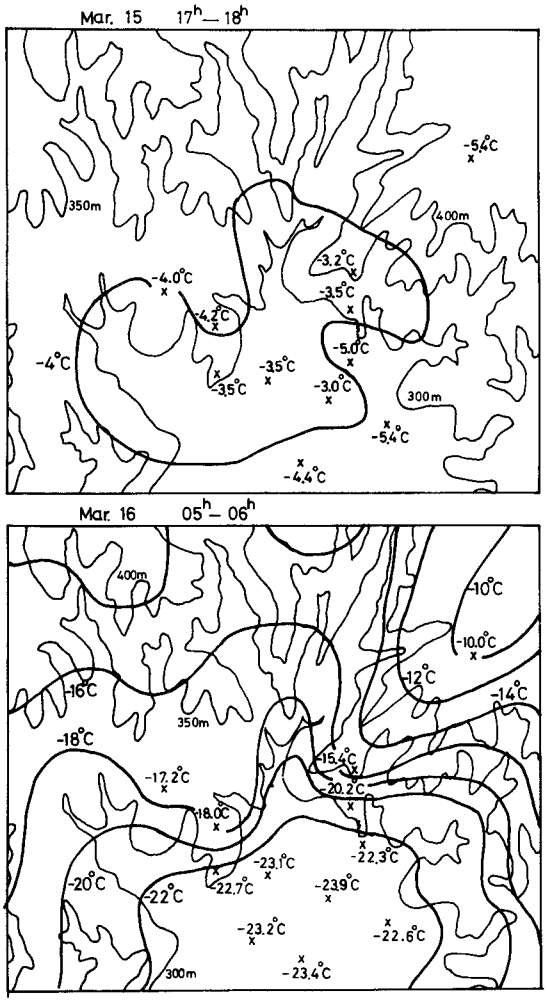

Fig. 3 Horizontal temperature distributions in Moshiri in winter.
Top : at sunset Bottom : at sunrise

interval of contour lines is 50 m in altitude. One can see that a homogeneous temperature distribution (−4 to −5°C) appears throughout the whole area immediately after sunset and that a large temperature difference is observed immediately before sunrise with an increase in height especially in winter (Fig.3). While the temperature drops below −25.5°C at the lower part of the basin, it remains about −10°C at the higher part. There is a temperature inversion of about 15°C between these two parts. The same tendency can also be found in the snow-melting season (Fig.4), during which the inversion strength is about 8°C, only a half of that observed in winter. Evidently in both the

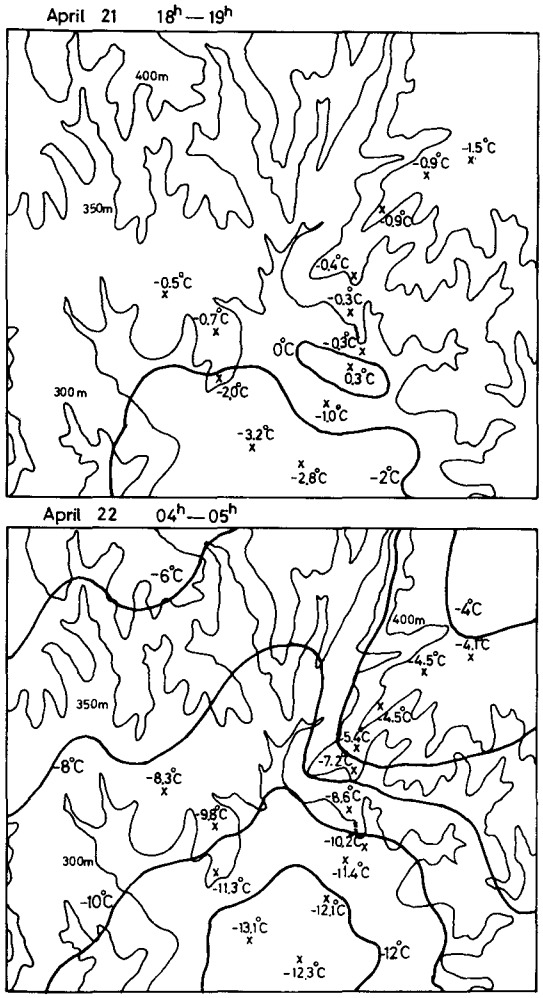

Fig. 4 Horizontal temperature distributions in Moshiri in the snow-melting season.
Top : at sunset Bottom : at sunrise

seasons the horizontal temperature difference is very small throughout the whole lower part of the basin. It can be said from the foregoing that the values observed at the lower station stand for the values representing the bottom of the basin and that an influence by horizontal advection counts for little because of a very small difference in horizontal

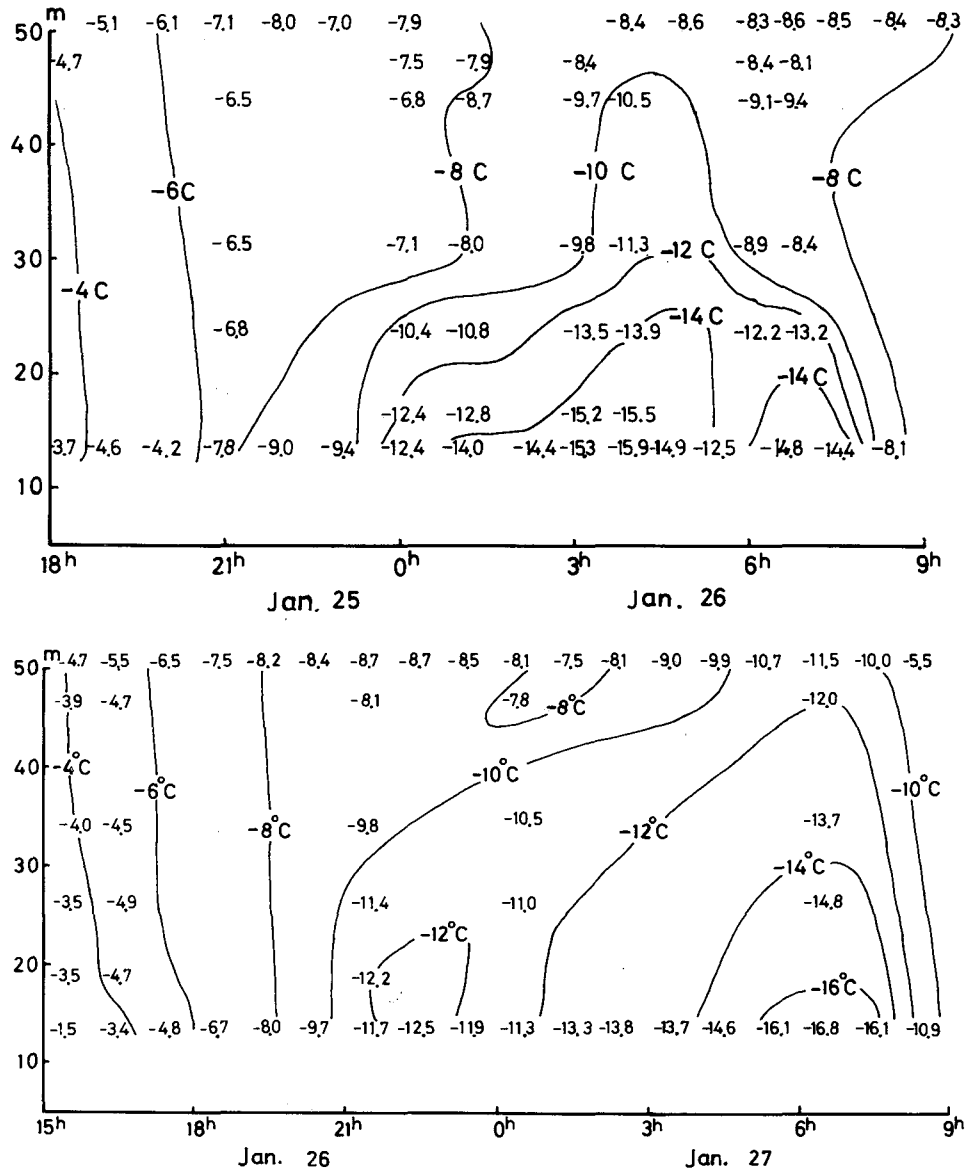

Fig. 5(a) and (b) Variations of isotherm with time along a mountain slope. Interval of contour lines : 2°C.

temperatures.

The vertical temperature profile along a mountain slope was examined much more in detail. Figures 5 (a) and (b) show the variations of isotherm with time (isopleth). From 1800 to 2000 hours in the evening there is no temperature difference with height, but early in the morning the air temperature gradually decreases down to −16°C at the lower station. On the other hand, during the night the decrease of temperature is not so large at the higher station. The maximum temperature inversion strength between two altitudes with a difference of 40 m was found to be 7°C in the observational period. It is shown in these figures that the cold air might constitute a lake filling the lower part of the basin, but a temperature decrease occurs earlier at the lower station than at the higher station. It cannot be said from this isopleth that a cooled air mass flows down constantly over the slope. Finally a temperature inversion disappears within several hours after sunrise.

(3) *Air temperatures near a mountaintop*

From the observational results, it is clear that the air temperature at the higher station does not change very much during the night when radiative cooling is dominant. The strength of inversion ΔT and the air temperature near a mountaintop are plotted in Fig.6, which shows no distinct relation between them. The temperature is not so low,

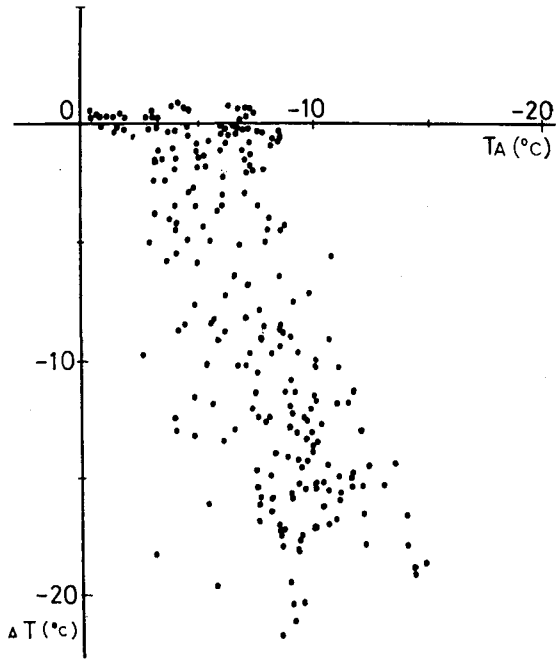

Fig. 6 Relation between inversion strength ΔT and air temperature T_A at mountain top.

reaching around −15°C at the lowest degree. The author calls this air temperature near a mountaintop the normal-current air temperature. With a view to examining the air temperature over the island of Hokkaido during winter, the isopleths based on radiosonde data that were taken by Sapporo Meteorological Observatory are shown in Fig.7. The

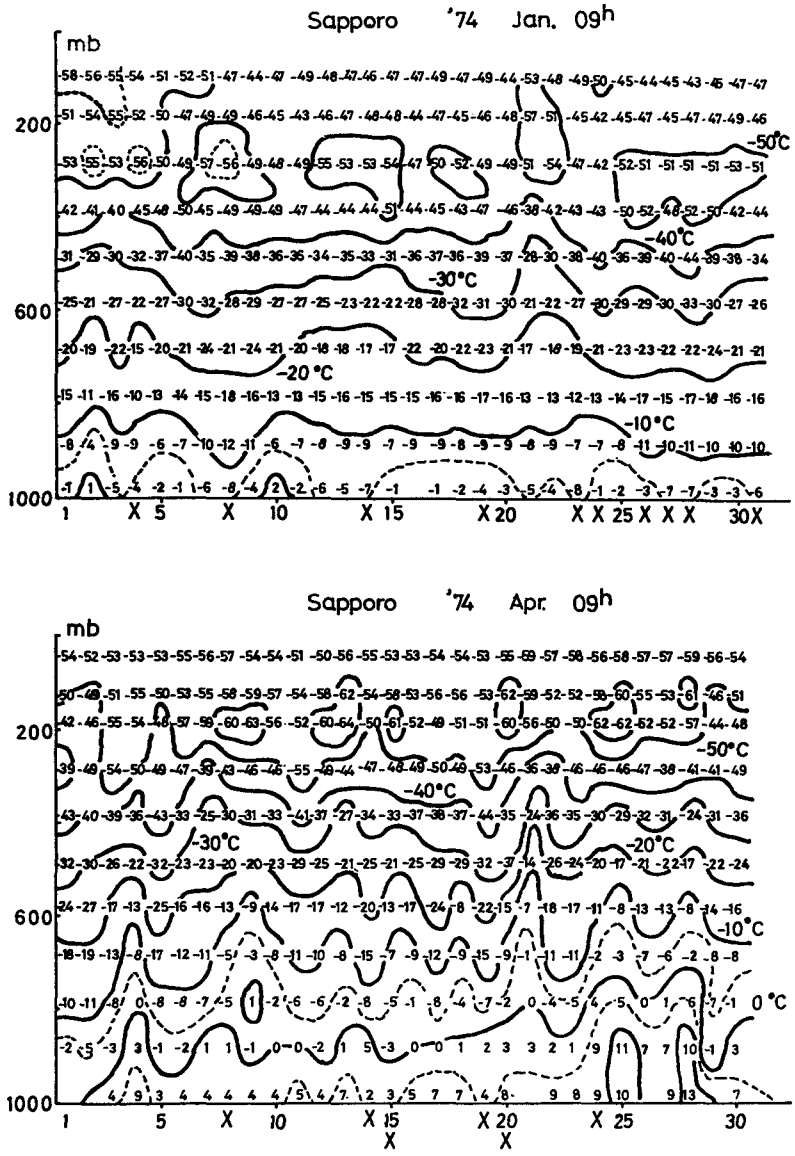

Fig. 7 Isopleths using sounding data over Sapporo.
X : days when remarkable radiative cooling occurred.

cross mark (x) on the bottom of this figure shows the day when remarkable radiative cooling occurred in Moshiri. It can be said that the air mass with extremely low temperatures did not necessarily cover the island on the cross-marked days. Figure 8 shows the monthly average of vertical temperature profiles in January, Feburary and April. At a 200 mb height it is colder in April than in midwinter. In spite of this result it happens that more remarkable radiative cooling occurs near the ground in winter than in the snow-melting season. From this figure it is reasonable to take −55 to −65°C as temperatures of the tropopause over the island during winter. Therefore, if the lapse rate of the standard atmosphere −0.65°C/100 m is used, the values of −3 to −13°C are

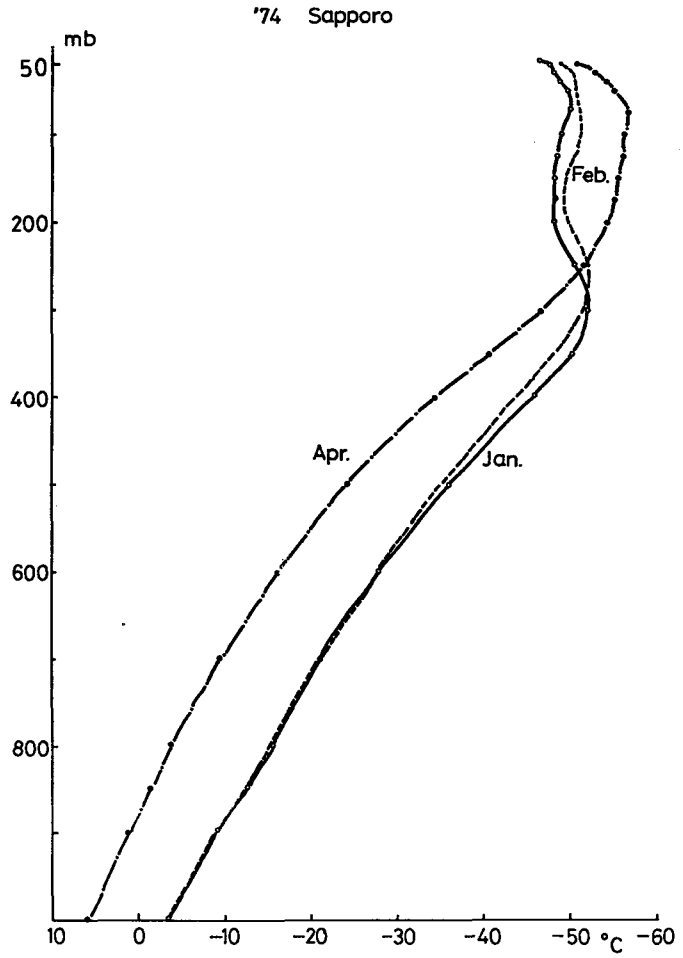

Fig. 8 Monthly mean vertical temperature profiles in Sapporo.

calculated as temperatures near the ground. They are equal to the normal-current air temperature measured near the mountaintops surrounding the basin. Namely, normal-current air temperatures in low altitudes above sea level in this island during winter might be about −15°C at the lowest degrees, while air temperatures below them might not be brought about by an inflow of a large scale cold air mass but by local cooling.

(4) *Weather conditions and duration of radiative cooling*

Weather conditions which constitute causes for radiative cooling are shown in Fig. 9. Durations of radiative cooling are shown by black arrows, whereas each one of the marks representing meteorological elements is expressed as an average of the element observed every six hours. It can be said that radiative cooling occurs during a calm clear night, not in a cloudy or snowy day. Figure 10 shows the time variation of the elements during observational periods in winter and the snow-melting season at Moshiri. The notation $\Sigma\Delta R$ stands for the total sum of net radiation amount in cal/cm^2 which is measured at the lower station for 12 hours from 1800 to 0600 hours. The notation ΔT shows the difference of the minimum temperature at a 1 m height above the snow surface at the higher and the lower station. The notation V stands for the mean wind speed in m/s from 1800 to 0600 hours. Solid lines show values at the higher station and broken lines values at the lower station. In winter (in Moshiri) a large temperature inversion occurred when the radiative heat loss was large and the wind speed was relatively low. The wind speed measured was always higher at the higher station than at the lower station. In the snow-melting season, although the same tendency occurs, the inversion strength ΔT was not so large as compared with the one in winter.

The probability and duration of radiative cooling measured in Toikanbetsu are shown in Fig. 11. The abscissa represents the time, while the ordinate represents the occurrence probability, namely, for a period from January to March during the three

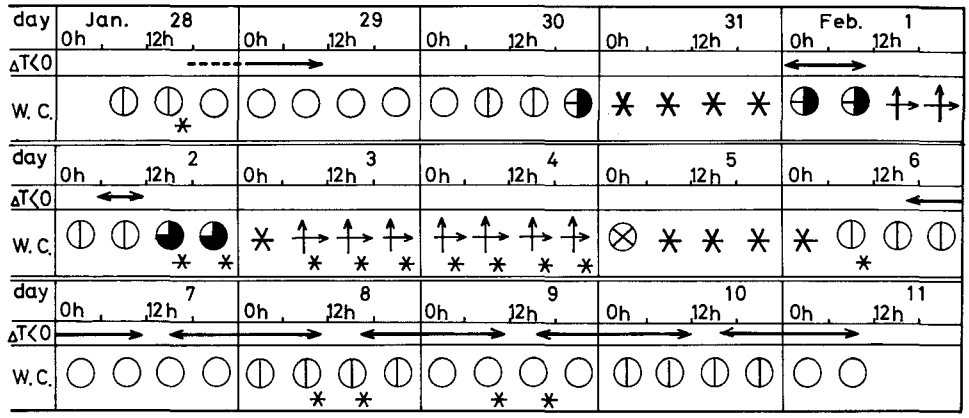

Fig. 9 Weather conditions and durations of radiative cooling.

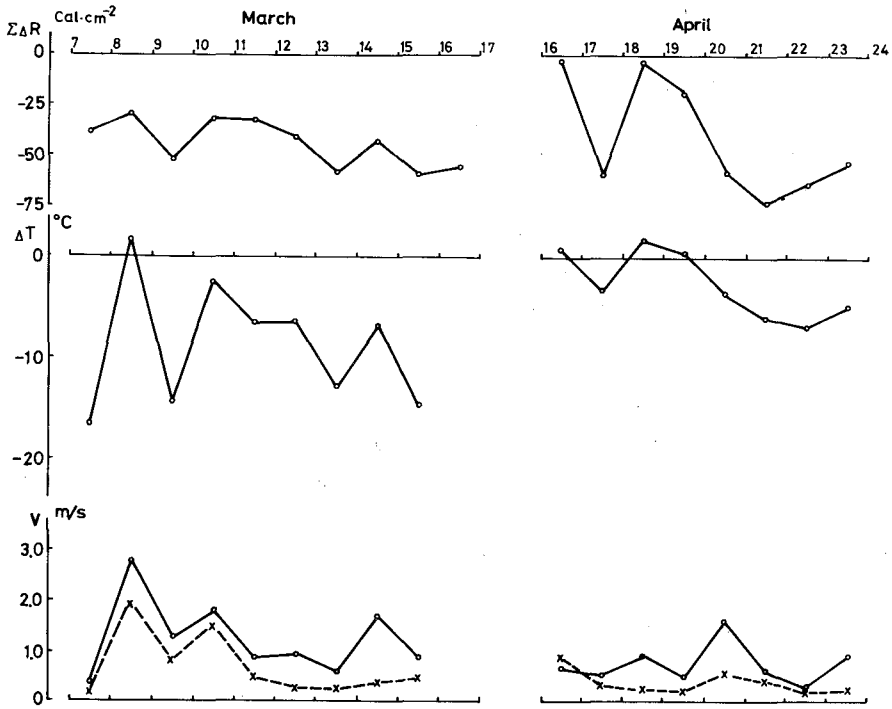

Fig. 10 Variations of meteorological elements in Moshiri
$\Sigma\Delta R$: amount of net radiation, ΔT : difference of minimum 1 m height temperature between higher and lower stations, V : mean wind speed

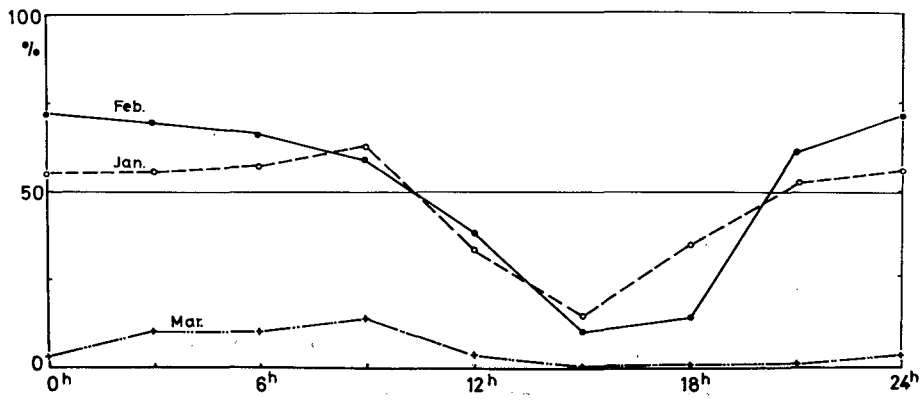

Fig. 11 Probability and duration of radiative cooling

years, the number of such inversions that take place during one-hour interval (i. e., when ΔT becomes negative) is shown by a percentage against the total number of hours. In Toikanbetsu inversions occur in January and February at the probability over 50% from evening to morning (2000 to 1000 hours), but they almost diminish in the afternoon. Inversions which occur frequently at night disappear during the daylight time in case of Hokkaido due to solar radiation. But in polar regions such an inversion lasts for a week or so because no solar radiation takes place in winter, whereby a strong ground inversion layer develops (WENDLER and JAYAWEERA 1972).

(5) *Relation between inversion strength and wind speed*

It was mentioned earlier that calmness of winds was a condition necessary to bring about radiative cooling in a land basin. Air temperatures and wind speeds measured at the higher and the lower station are plotted in Fig. 12 with an aim to confirm if there is any relation between them. In this figure the abscissa represents air temperatures and the ordinate wind speeds; open circles show values at the higher station and cross marks those at the lower station. When wind speeds measured at the lower station become below 2.5 m/s, and extremely low temperature such as −30°C or under is observed, while at the same time a relatively high temperature appears at the higher station. At a mountaintop high wind speeds are measured usually, compared with them at the lower parts of the basin. Although calm winds happen to appear sometime also at the higher parts of the basin, extremely low temperatures are never observed there, the reason for which will be discussed in detail later (in section V-2).

Figure 13 shows a relation between the inversion strength ΔT and wind speed. It

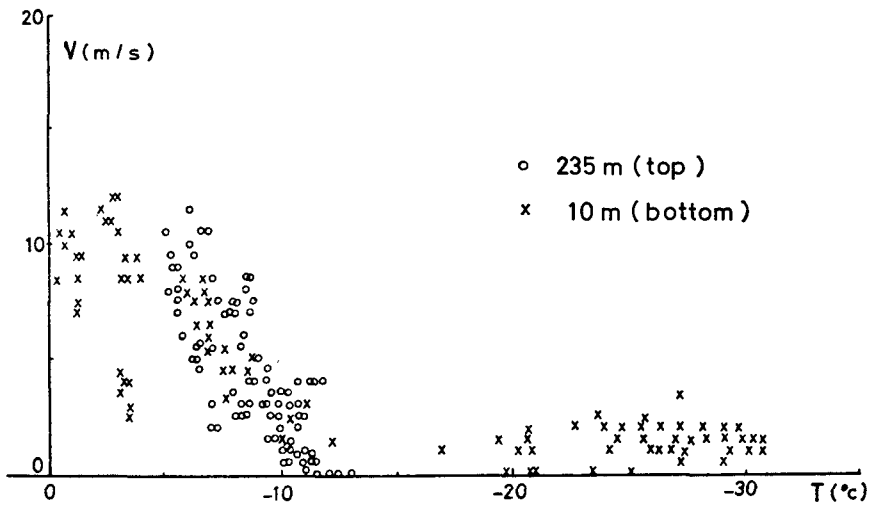

Fig. 12 Relation between wind speed (V) and air temperature (T)

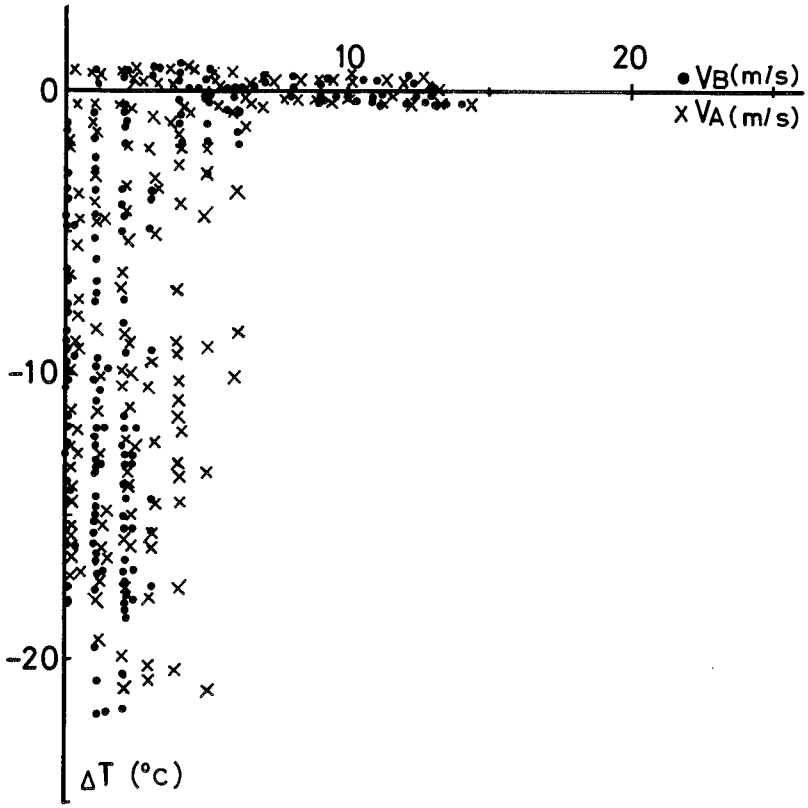

Fig. 13 Variations of intensity of inversion (ΔT) with wind speed (V).
● : wind speed (V_B) at a lower station
x : wind speed (V_A) at a higher station

can be again said that, when a wind speed at the lower station becomes lower, a greater inversion occurs, but, when it exceeds 2.5 m/s, an extensive inversion is not observed. Even when a wind speed is relatively high in the value of about 5 m/s or above at a mountaintop, a strong inversion is found to take place. After all, when wind speeds at the lower part become considerably low, a low temperature appears there and a great temperature difference is observed between the lower and the higher part of the basin. This is a phenomenon of radiative cooling. Figure 14 shows a relation between the wind speed measured at the lower station V_B and the strength ΔT of an inversion which occurs when the wind speed is low at the bottom of the basin during both winter and the snow-melting season, the strength of inversion being smaller in the latter.

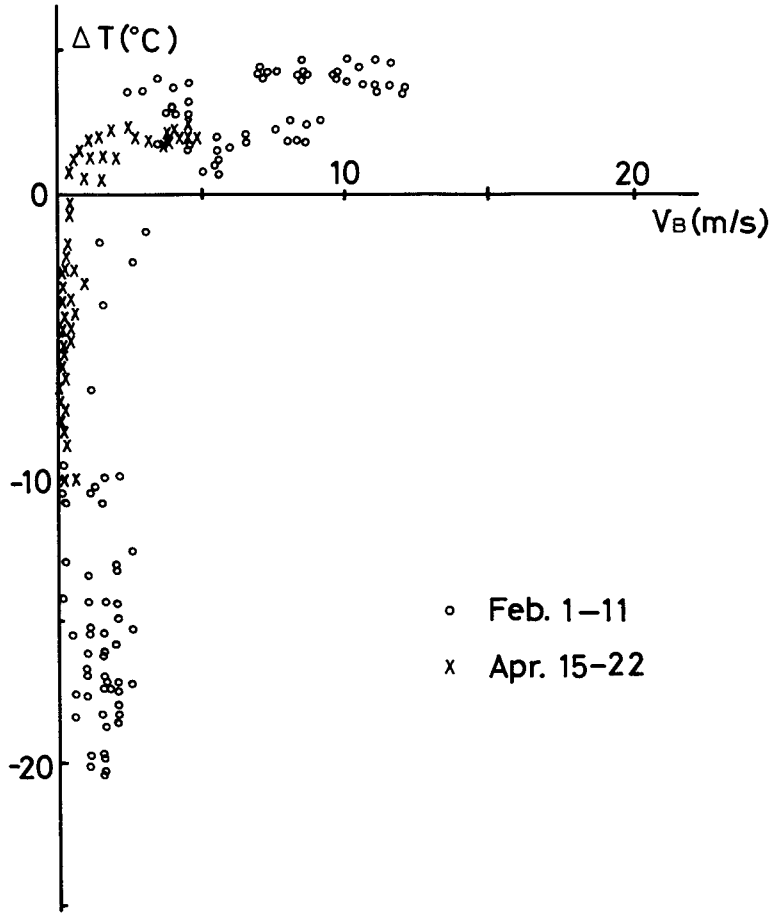

Fig. 14 Seasonal variations of intensity of inversion ΔT with wind speed at lower station V_B.
o : winter,
x : snow-melting season

(6) *Air temperatures at a land basin and a mountaintop*

It was shown earlier that T_B, the air temperature variation measured during the night at the bottom of a basin, was much greater than T_A, that at a mountaintop. A relation between T_B and T_A is plotted in Fig. 15, where the ordinate represents T_B(°C) and the abscissa T_A(°C). In this figure the straight line M-M' shows the case that $T_B = T_A$, which means the temperatures at both stations are equal. The region below the line M-M', where T_B is lower than T_A, is defined in this paper as being in the state of temperature inversion. The line K-K' represents the relation $T_B = 2 + T_A$, which means that the air temperature at a mountaintop with a 250 m height difference de-

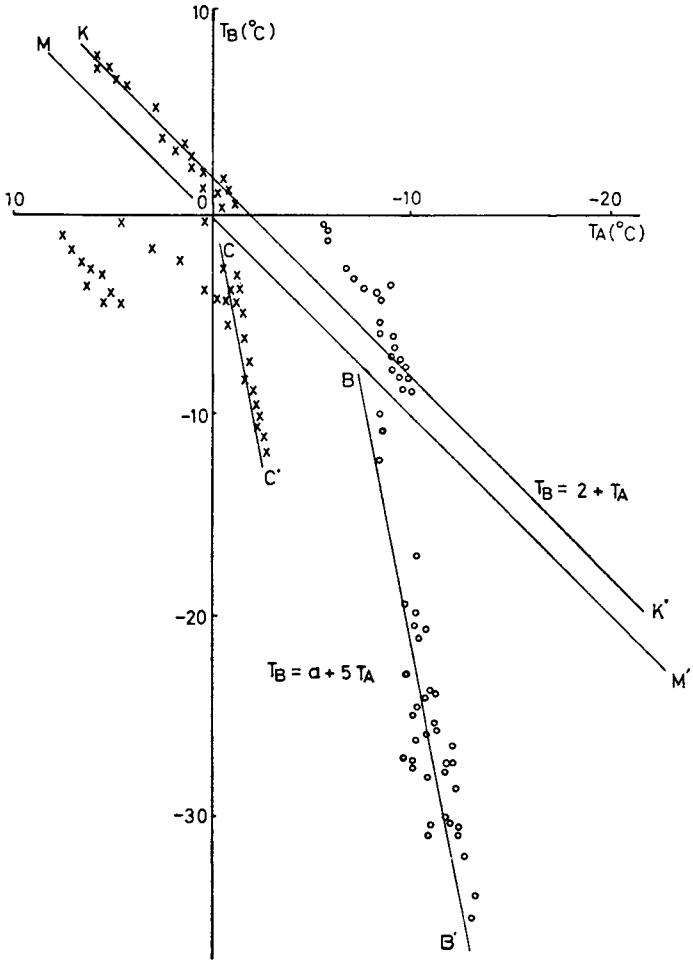

Fig. 15 Relations between air temperatures at two stations T_A and T_B.
o : winter,
x : snow-melting season

creases with dry adiabatic lapse rate. When no inversion occurs, the relation of temperatures between the two stations fits this line. The temperature difference during the radiative cooling can be expressed by the line B-B' for winter and C-C' for the snow-melting season. These lines can be expressed by the following equation: $T_B = a + 5T_A$. After differentiation of this equation with respect to time, $\frac{\partial T_B}{\partial t} = 5\frac{\partial T_A}{\partial t}$ is derived. From this fact it might be said that when radiative cooling takes place, the changes of air temperature at the bottom are five times as large as those at the mountaintop. Whenever T_A is above 0°C, an inversion also occurs, but compared with the

case when the temperature is below 0°C, a temperature variation at the lower station is not so large. The reason for it will be discussed later (in section III—2—c)

(7) *Amount of long-wave radiation and surface temperature*

The upward long-wave radiation $Q_L\uparrow$ from the snow surface is directly obtained by using a radiometer set up just near the surface. Also σT_o^4 is calculated by measuring

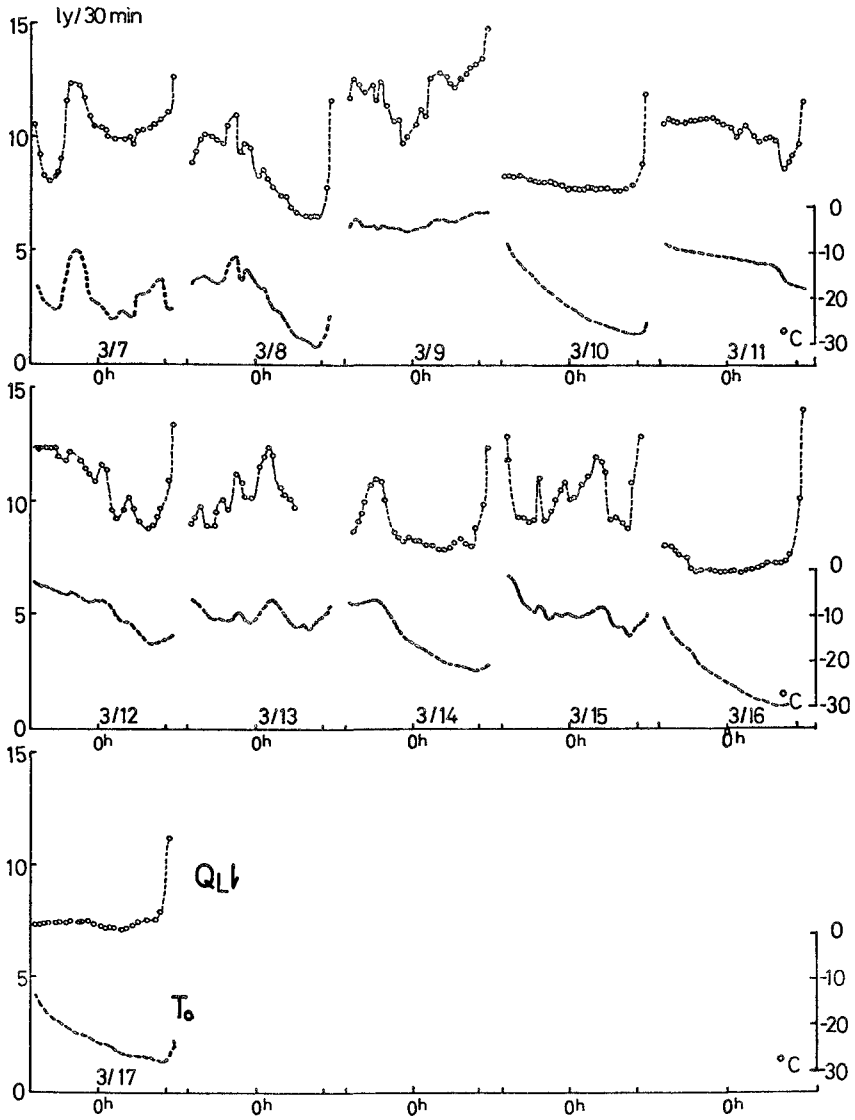

Fig. 16 Time variations of atmospheric radiation $Q_L\downarrow$ and surface temperature T_o in winter.

the snow surface temperature T_0, where σ is the Stefan-Boltzmann constant. Comparison between the values of $Q_L\uparrow$ and σT_0^4 shows that they are in good agreement. Therefore, the snow cover can be assumed to be a black body as far as long-wave radiation is concerned. Yet, when a radiometer is placed at a level at some distance above the surface, the values of σT_0^4 and $Q_L\uparrow$ happen to disagree sometimes due to radiation absorption or divergence in an air layer between the snow surface and the radiometer (FUNK 1960, IDSO and COOLEY 1971, KONDO 1972). Figures 16 and 17 show the time variations of $Q_L\downarrow$ which denotes the downward long wave radiation from the sky measured with a radiometer, and of T_o in winter and the snow-melting season, respectively. Evidently low temperatures appear when $Q_L\downarrow$ has a constant low value during the night. Although $Q_L\downarrow$ has a high constant value sometimes, it is due to back radiation from a cloud base in an overcast night, and under such a condition the surface temperature becomes 0°C. Using an empirical equation (KONDO 1967), the amount of atmospheric radiation is about 7 cal cm^{-2} $(30min)^{-1}$ in a clear night with the air temperature of −15°C and the vapor pressure of 4 mb, while, the amount of back radiation from a cloud base with the air temperature of 0°C is about 13.8 cal cm^{-2} $(30min)^{-1}$.

The heat energy gained by the snow surface is due not only to atmospheric radiation but also to the sensible or latent heat transferred from the air immediately above the surface. But one can see from these figures that the variation patterns of atmospheric radiation and magnitude of these values are very similar to the variation patterns of snow surface temperature and amount of its decrease. Namely, $Q_L\uparrow$ changes so that it balances $Q_L\downarrow$; as a result, the surface temperature may change. In the snow-melting season $Q_L\downarrow$ becomes larger, but a decrease of T_0 is smaller compared with that in winter. Table 1 shows the values of $Q_L\downarrow$, $Q_L\uparrow$ and $Q_N(=Q_L\downarrow-Q_L\uparrow)$, namely the amount of net radiation, which were measured at the higher and the lower station. These values were

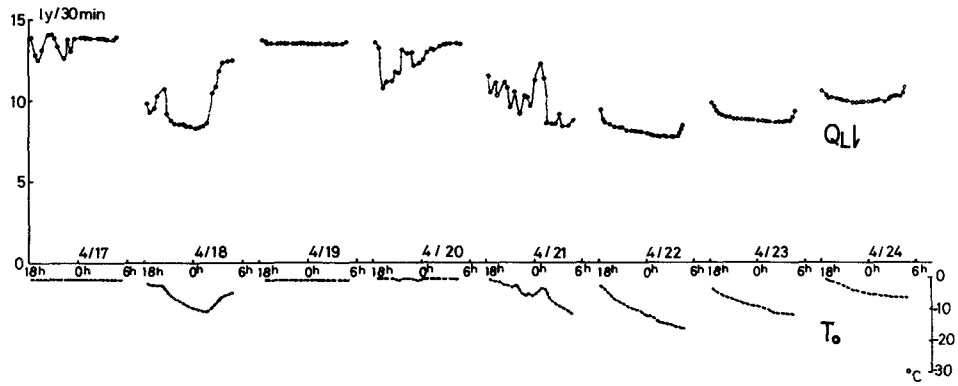

Fig. 17 Time variations of atmospheric radiation $Q_L\downarrow$ and surface temperature T_o in snow-melting season.

Table 1 Comparison of amounts of long-wave radiations between higher and lower meteorological stations.

Date	Higher Station			Lower Station		
	$Q_L\uparrow$	Q_N	$Q_L\downarrow$	$Q'_L\uparrow$	Q'_N	$Q'_L\downarrow$
Feb. 2 – 3	− 297.5	− 5.1	292.4	− 308.0	− 8.5	299.5
Feb. 3 – 4	− 304.8	− 6.3	298.5	− 322.8	− 5.4	317.4
Feb. 4 – 5	− 297.6	− 6.0	291.6	− 316.8	− 7.0	309.8
Feb. 5 – 6	− 290.4	− 34.8	255.6	− 294.0	− 16.8	277.2
Feb. 6 – 7	− 276.0	− 42.2	233.8	− 235.2	− 26.4	208.8
Feb. 7 – 8	− 275.5	− 74.8	200.7	− 210.1	− 19.7	190.4
Feb. 8 – 9	− 280.8	− 75.6	205.2	− 222.3	− 21.6	200.7
Feb. 9 – 10	− 280.2	− 74.4	205.8	− 220.8	− 28.8	192.0
Feb. 10 – 11	− 277.2	− 54.5	222.7	− 225.6	− 38.4	187.2

measured in cal/cm² for an observational period of 12 hours at night. No inversion occurred before Feb. 6, after which a strong inversion occurred. During the inversion period, $Q_L\downarrow$ was larger at the higher station than at the lower station. This is because $Q_L\downarrow$ through a cold air layer might have been slightly smaller than $Q_L\downarrow$ from the mean air flow with a relatively high temperature. On the other hand, the difference of $Q_L\uparrow$, which depends upon the difference of temperatures between the two stations, was much larger than the difference of $Q_L\downarrow$. Therefore, the absolute value of Q_N was larger at the mountaintop than at the bottom of the basin. This means that an energy loss due to radiation at the higher station is larger than at the lower station.

III — 2 *Heat balance during radiative cooling*

Radiative cooling observed at a land basin resulted from local cooling of an air mass, which had different temperatures in different seasons as mentioned before. Furthermore, winter and the snow-melting season had different strengths of temperature inversion even if they had the same wind conditions. Therefore, using meteorological elements observed at the higher and the lower station for both seasons, the heat balance components were obtained when radiative cooling took place, whereby they were examined about how they were related with the inversion strength. In this section a heat balance is estimated on the snow surface, so the temperature which will be obtained from the heat balance will represent the surface temperature. If the influences of advection and divergence of radiation in the air are assumed to be negligible, it is considered that a change in the surface temperature is transmitted by diffusion into the air and the snow cover. Therefore, a discussion is made in this section mainly of the surface temperature variations.

III—2—a *Heat balance in winter*

In winter, when a snow cover does not contain meltwater, a heat balance in the snow cover per unit area is described by the following equation (MUNN 1966) :

$$Q_N + Q_T + Q_E + Q_C = 0 \tag{1}$$

where the fluxes toward the surface are regarded as positive and those fluxes away from the surface as negative, Q_T is the sensible heat flux, Q_E the latent heat flux of evaporation or condensation, and Q_C the conductive heat flux in the snow cover.

(1) *Nocturnal radiation balance*

The radiation balance Q_N on the snow surface is represented as

$$Q_N = Q_L\downarrow - Q_L\uparrow + Q_S\downarrow - Q_R\uparrow \tag{2}$$

where $Q_S\downarrow$ is the incoming short-wave radiation and $Q_R\uparrow$ the reflected short-wave radiation. Then $Q_L\uparrow$ is approximately represented by

$$Q_L\uparrow = \varepsilon\sigma T_o^4 + (1 - \varepsilon)\, Q_L\downarrow \tag{3}$$

Since the snow cover is nearly a black body respecting long-wave radiation, the emissivity ε can be put to be unity. Consequently eq.(3) becomes

$$Q_L\uparrow = \sigma T_o^4 \tag{3}'$$

Short-wave radiation is diminished during the night, so the nocturnal radiation balance can be shown as

$$Q_N = Q_L\downarrow - Q_L\uparrow = Q_L\downarrow - \sigma T_o^4 \tag{2}'$$

In this study, Q_N can be obtained from a direct measurement using a net radiometer or from $Q_L\downarrow$ and $Q_L\uparrow$ which are obtained by GARP-type radiometers.

(2) *Sensible heat transfer*

For logarithmic profiles of air temperature and wind speed, the sensible heat flux is given by

$$Q_T = \rho_a C_p K_a \frac{dT}{dZ}\, t \tag{4}$$

where C_p is the specific heat of air, K_a the thermal diffusivity, ρ_a the density of air and t the time.

The coefficient K_a is obtained from the relation :

$$K_a = u_* k (Z + Z_0) \tag{5}$$

where u_* the friction velocity and k the von Kārmān constant. A correction (LETTAU 1949, WELLER 1968) for non-adiabatic conditions is made by using

$$K=K_a/(1+X)^2 \tag{5}'$$

where K is the thermal diffusivity for non-adiabatic conditions and X a stability criterion as shown like

$$X=\frac{gk^2(Z+Z_0)^2}{T\cdot u_*^2}\frac{d\theta}{dZ} \tag{6}$$

where g is the gravitational acceleration and θ the potential temperature.

The sensible heat flux was actually obtained by measuring the air temperatures T_1, T_0 and the wind speeds V_1, V_0 at the different heights Z_1, Z_0, respectively, and using the following equation which is derived from eqs. (4),(5) and (5)′

$$Q_T=\rho_a C_P k^2\frac{V_1-V_0}{ln\,Z_1/Z_0}\frac{T_1-T_0}{ln\,Z_1/Z_0}\frac{1}{(1+X)^2} \tag{4}'$$

(3) *Latent heat transfer*

The evaporation or condensation amount E_V is obtained from the equation :

$$E_V=\rho_a k^2\frac{0.623}{P}\frac{V_1-V_0}{ln\,Z_1/Z_0}\frac{e_1-e_0}{ln\,Z_1/Z_0}\frac{1}{(1+X)^2} \tag{7}$$

where P is the atmospheric pressure, e_1 and e_0 the water vapor pressures at Z_1 and Z_0, respectively. Since the air immediately on top of the surface of a snow cover is usually considered to be saturated with respect to ice, e_0 is taken as an ice saturation vapor pressure at that temperature. The latent heat flux is estimated from eq. (7) multiplied by the latent heat of evaporation.

(4) *Amount of heat in a snow cover*

The conductive heat flux in a snow cover Q_C represents the amount of heat exchange between a snow surface and a snow cover lying underneath. Considering a unit column of the snow cover, Q_C is the sum of the amounts of horizontal heat exchange and of heat storage variation of its column with a depth of Z. But the former term is usually very small ; therefore

$$Q_C=\rho C\int_0^Z\frac{\partial T}{\partial t}dZ \tag{8}$$

where ρ is the density of snow and C the specific heat of ice.

III—2—b *Heat balance in the snow-melting season*

In the snow-melting season, a snow cover contains liquid water which is made during the daytime with an air temperature above 0°C. Therefore, the snow cover has a temperature of 0°C throughout the layer, wherein no heat flux by conduction exists. But losing a heat energy from the surface during the night, this liquid water refreezes and a crust layer develops. Consequently for the heat balance in the snow-melting season it must be considered that the amount of latent heat due to this phase changes.

Therefore, Q_C of eq. (1) is reduced to

$$Q_C=\rho C\int_0^{Z^*}\frac{\partial T}{\partial t}dZ+\rho WL_i\left(\frac{\partial Z^*}{\partial t}\right) \tag{9}$$

where Z^* is the depth of a crust layer, W the liquid water contents, and L_i the latent heat of refreezing.

Actually $Q_L\downarrow$ and $Q_L\uparrow$ are measured by using radiometers ; Q_T and Q_E are estimated from the profiles of air temperature, wind speed and water-vapor ; Q_C is obtained from the profiles of snow temperature or by heat-flow meters.

III—2—c *Heat balance during radiative cooling*

(1) *Heat balance at a land basin in winter*

Each component of the heat balance at the lower station is given diagrammatically on a daily basis in Fig. 18 for a period from Jan. 23 to Jan. 27, 1976. The values of each component are summed up from 1700 to 0700 hours, i. e., for a total of 14 hours at night. From Jan. 23 to Jan. 26 intensive radiative cooling occurred, but on Jan. 27 it did not. It is shown clearly that a negative heat supply to the surface is due to long-wave radiation and that, on the other hand, a positive heat supply is due to a turbulent transfer of sensible and latent heat, though their values are relatively small, especially in case of the latter. Choosing the days when the intense radiative cooling occurs, the percentages of each component to the total heat supply or heat loss are represented in Fig. 19. The ordinate at the right-hand side of this figure expresses the heat balance components in langley per hour. In this figure R denotes the net radiation amount, S the sensible heat,

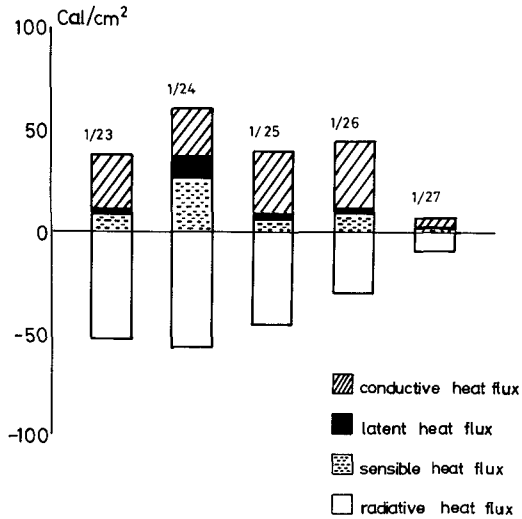

Fig. 18 Daily values of heat balance components at a lower station in winter.

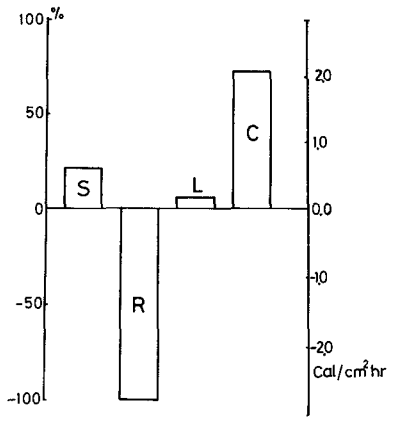

Fig. 19 Mean values of heat balance during radiative cooling in winter.

L the latent heat of evaporation or condensation, and C the change in heat storage amount of a snow cover. It is seen that 23 % accounts for a sensible heat flux and 6 % a latent heat flux, but they cannot compensate for a heat loss due to radiation (−100 %); consequently, the snow cover loses heat resulting in the lowering of its temperature.

(2) *Comparison of heat balance in winter between a basin and mountaintop*

Heat balances at the two stations during winter are shown in terms of percentage components in Fig. 20. This is an example of observations in January, 1972, where the left-hand side shows values at the bottom of a basin (lower station) and the right-hand side those at the mountaintop (higher station). Also numerical amounts of heat of each component during the observational period are given in this figure. It can be seen that, while a cooling component at the two stations is only by a radiative process, the amount at the lower station is a half of that at the higher station. This heat loss is compensated by sensible heat (82 %) and latent heat (3.4%) at the higher station, and by sensible heat (38%) and latent heat (0.2 %) at the lower station. Consequently, differences between the positive and negative heat amounts (about 14 % at the higher station and 62 % at the lower station) are lost from the snow cover. From these results it can be said that the main heating component at the two stations is a sensible heat flux, and that a latent heat flux is of no significance. Namely, at the mountaintop a heat loss due to nocturnal

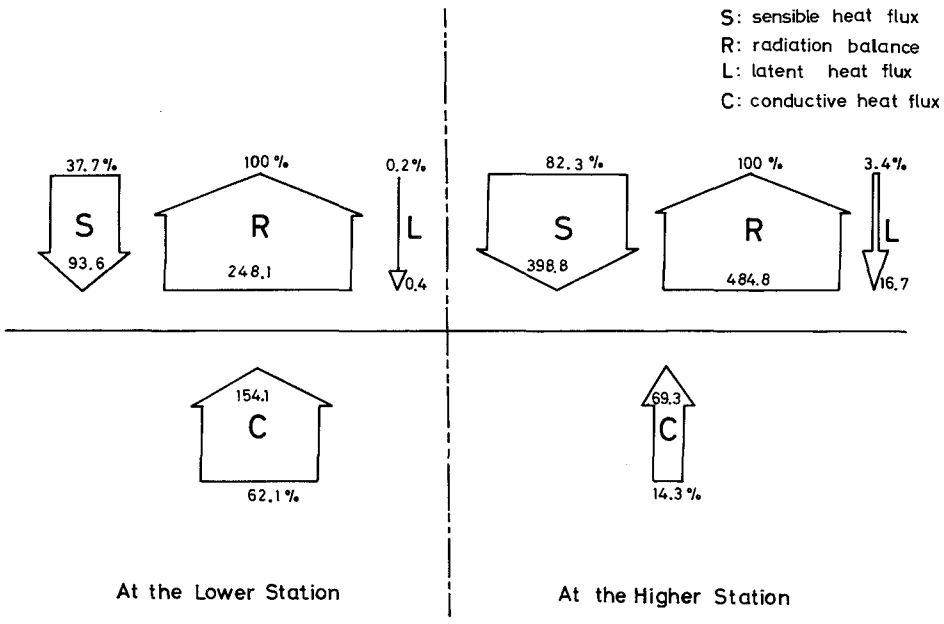

Fig. 20 Comparison of heat balance components during radiative cooling at two stations in winter.

radiation is larger than at the bottom of the basin, whereas a heat flux supplied to the snow surface from the turbulent air is also large; accordingly the total heat loss turns out to be so small that its temperature hardly drops.

(3) *Comparison of heat balance at a land basin between winter and the snow-melting season*

Seasonal changes of the components of heat balance at the lower station are shown in Fig. 21. These are results of observations in February and April in 1975. The same tendency described in the previous section is seen in this figure; namely, radiation constitutes the only heat sink and a sensible heat flux is the most important source for a heat balance at the surface during the period of a nocturnal temperature inversion. As compared with the heat balance in winter, that in the snow-melting season is marked by the main difference due to the latent heat flux released when melting water in a snow cover refreezes, which amounts to about 63 % of the total heat supply; as a result, the heat loss of the snow cover is as small as about 30 %. This is considered to be one of the causes of a weak inversion.

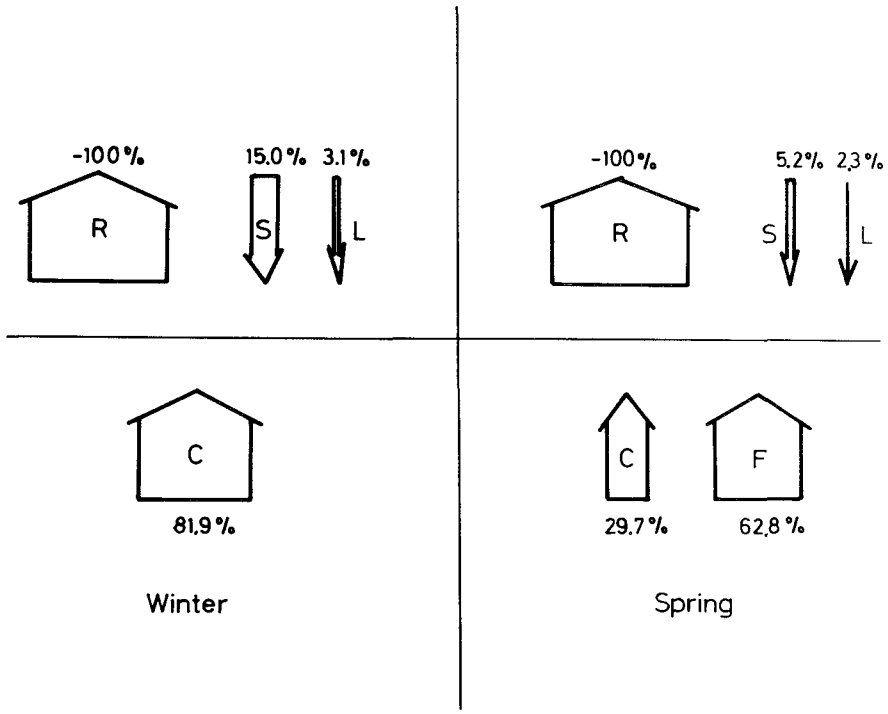

Fig. 21 Comparison of heat balance components at a lower station between winter and snow-melting season.

Ⅳ. Numerical temperature change with time near a snow surface

Variations of temperature and heat balance in winter and the snow-melting season are estimated in this section by numerical calculations. Based on observational results, the following model is used for calculation : A snow layer has a depth of 100 cm over the ground in both seasons,while an air layer with a constant temperature exists from the snow surface to the height of 250 m. This is based on the observational results that the variation of air temperature measured at the mountaintop with a 250 m height difference is small during the occurrence of radiative cooling. Furthermore, no radiative absorption is assumed in the air layer which is 250 m in thickness. A latent heat flux resulting from evaporation or condensation at the surface is neglected because of its small amount. It is also assumed that in the snow-melting season liquid water is distributed uniformly throughout the snow cover.

Ⅳ—1 *Calculational method*

A snow cover does not contain liquid water in winter, so the heat balance at the snow surface is represented by the equation :

$$Q_N+Q_T+Q_C=0 \tag{1}$$

where Q_N is the amount of net radiation, Q_T the sensible heat flux by turbulent transfer, and Q_C the conductive heat flux in the snow cover. The latent heat flux Q_E is neglected. Fluxes toward the surface will be regarded as positive and those away from the surface as negative. Each component of eq.(1) can be shown as follows :

$$Q_N=(1-\alpha_s)\,I_s+(1-\alpha_L)(I_L-\sigma T_0^4) \tag{2}$$

$$Q_T=\rho_a C_P K\left(\frac{\partial\theta}{\partial Z}\right)_{Z=Z'} \tag{3}$$

$$Q_C=-\lambda\left(\frac{\partial T}{\partial Z}\right)_{Z=0} \tag{4}$$

where I_s is the amount of solar radiation, I_L the amount of long-wave radiation, α_s and α_L the reflectivities of short and long-wave radiation, σ the Stefan-Boltzmann constant, T_o the surface temperature of a snow cover, C_p the specific heat of air, K the thermal diffusivity, θ the potential temperature, λ the heat conductivity of snow, and T the snow temperature.

Using empirical equations (KONDO 1967), I_s and I_L are derived as follows :

$$I_s=J_0\left(\frac{\overline{d}^2}{d}\right)\cos\zeta(0.3+0.7\times10^{-0.055(1+0.04e_H)\sec\zeta}) \tag{5}$$

$$\cos\zeta = \sin\varphi \sin\delta + \cos\varphi \cos\delta \cos h \tag{6}$$

$$I_L = \sigma T_H^4 (1-(0.49-0.066\sqrt{e_H})) \tag{7}$$

where J_o is the solar constant, $\bar{d}$ and d the mean and instantaneous distance between the sun and the earth, e_H the mean vapor pressure of an air mass with the temperature T_H, ζ the solar zenith angle, φ the latitude of an observational site, δ and h the solar declination and hour angle.

The temperature fields in the air and the snow cover are represented by the following equations (ZDANKOWSKY 1966, CARSLOW and JAEGER 1959),

$$\frac{\partial\theta}{\partial t} = \frac{\partial}{\partial Z}\left(K\frac{\partial\theta}{\partial Z}\right) \tag{8}$$

$$\frac{\partial T}{\partial t} = \frac{\lambda}{\rho C}\frac{\partial^2 T}{\partial Z^2} \tag{9}$$

where the thermal diffusivity K is the function of height and wind speed in a surface boundary layer (YAMAMOTO and SHIMANUKI 1966), but in this calculation the diffusivities introduced by LETTAU (1962) are used under performing corrections for stability. The heat conductivity of a snow cover is obtained by using the YOSHIDA'S equation (YOSHIDA and IWAI 1947).

In the snow melting season the following equation is used to represent the heat balance of the surface instead of eq. (1)

$$Q_N + Q_T + Q_C + Q_M = 0 \tag{1}'$$

where Q_M is the amount of latent heat released by a phase change in the snow cover, that is, freezing of meltwater (positive sign) and melting of snow (negative sign). In respect to the motion of liquid water in the snow cover YOSHIDA (1962) did excellent work. Actual observations showed that the liquid water content was 3-6 % at the front of a crust layer (15-20 cm in depth from the surface) early in the morning, which had remained almost constant during the night preceding it. Therefore, it might be reasonable to assume that the liquid water dose not move downward but keeps its position in the snow cover during the development of the crust layer. Before the crust layer grows, there is no temperature gradient in the snow cover because liquid water is contained throughout the snow cover.

If $Q_N + Q_T < 0$, the first crust layer develops. If liquid water contained in the crust layer refreezes entirely, then a temperature gradient appears in this crust layer. At the front of the layer another new crust layer is assumed to develop according to the temperature gradient which was made at the previous time interval. Namely,

$$\lambda\left(\frac{\partial T}{\partial Z}\right)_{z=z^*} \cdot \Delta t = \rho W L_i \left(\frac{\partial Z^*}{\partial t}\right) \cdot \Delta t \tag{10}$$

where Δt is the time interval of calculation, W the water content, L_i the amount of latent heat due to refreezing of liquid water, and Z^* the thickness of a crust layer. Choosing the boundary and initial conditions to fit each observational fact, eqs. (8) and (9) are solved numerically. Putting i and j as time and space indexes, respectively, the numerical equations which are used in this calculation are the same as those introduced by MAYKAT (1969). Namely, the air temperature at position j th at time i th is obtained by

$$\bar{\theta}_j^i = \frac{\theta_i^{i-1} + \frac{2\Delta t}{\Delta Z_{j+1} + \Delta Z_j}\left\{\frac{K_j^{i-1}}{\Delta Z_j}\left(\theta_{j-1}^{i-1} - \theta_j^{i-1}\right) + \frac{K_{j+1}^{i-1}}{\Delta Z_{j+1}}\bar{\theta}_{j+1}^i\right\}}{1 + \frac{2\Delta t K_{j+1}^{i-1}}{(\Delta Z_{j+1} + \Delta Z_j)\Delta Z_{j+1}}} \tag{11}$$

It is clearly shown from this equation that, once putting a value into $\bar{\theta}_n^i$, which represents the upper boundary temperature at time i th, and making a change of j from n-1 to 1, then one gets the values of θ until $\bar{\theta}_1^i$. Furthermore, the following equation is used :

$$\hat{\theta}_j^i = \frac{\theta_j^{i-1} + \frac{2\Delta t}{\Delta Z_{j+1} + \Delta Z_j}\left\{\frac{K_{j+1}^{i-1}}{\Delta Z_{j+1}}\left(\theta_{j+1}^{i-1} - \theta_j^{i-1}\right) + \frac{K_j^{i-1}}{\Delta Z_j}\hat{\theta}_{j-1}^i\right\}}{1 + \frac{2\Delta t K_j^{i-1}}{(\Delta Z_{j+1} + \Delta Z_j)\Delta Z_j}} \tag{12}$$

Once getting the value of $\hat{\theta}_0^i$, which represents the surface temperature at time i th, and making a change of j from 1 to n-1, then one gets the values of θ until $\hat{\theta}_{n-1}^i$. The same equations are used for snow temperature distribution.

The mean value calculated from eqs. (11) and (12)

$$\theta_j^i = \frac{\bar{\theta}_j^i + \hat{\theta}_j^i}{2} \tag{13}$$

is taken as the air temperature at position j th at time i th.

The initial time of calculation is the time when the amount of total radiation becomes zero.

Ⅳ—2 *Results of calculation*

(1) *Variations of air and snow temperatures with time in winter and the snow-melting season*

The examples of calculational results are shown in Fig.22 (for Feb.7-8) and Fig.23 (for Apr.15-16). The numerical conditions for winter are: At the roughness height of 0.1 cm, the initial temperature is −15°C, wind speed 0.0m/s, albedo of snow 0.75; at the height of 250 m, the air temperature is −10.0°C, wind speed 3 m/s, vapor pressure 1.75 mb; the initial temperature profile of a snow cover is represented by $T(z) = -15.0 \exp(0.069Z)$ $(Z \leqq 0)$. The numerical conditions for the snow-melting season are: At the roughness height of 0.1 cm, the initial temperature is 0.0°C, wind speed 0.0 m/s, albedo of snow 0.65; at the height of 250 m, the initial temperature is 5.0°C, wind speed 3.0 m/s, vapor pressure 3.84 mb; the initial temperature profile of a snow cover is represented by $T(z) = 0.0$°C, its liquid water content being 10 %.

The following are the values used in this calculation common to winter and the

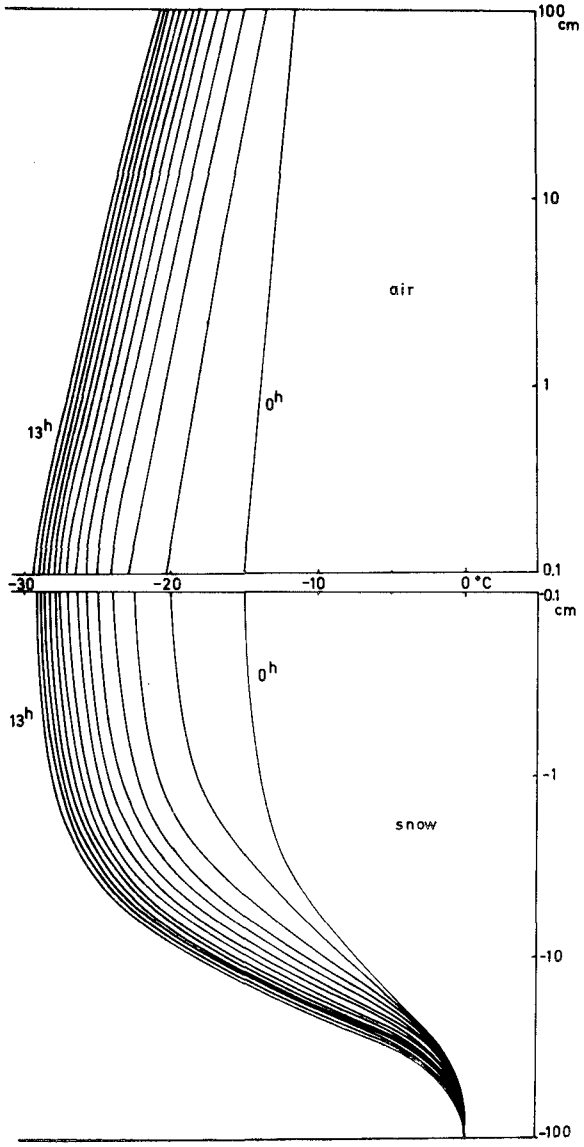

Fig. 22 Numerical variations of snow and air temperatures in winter.

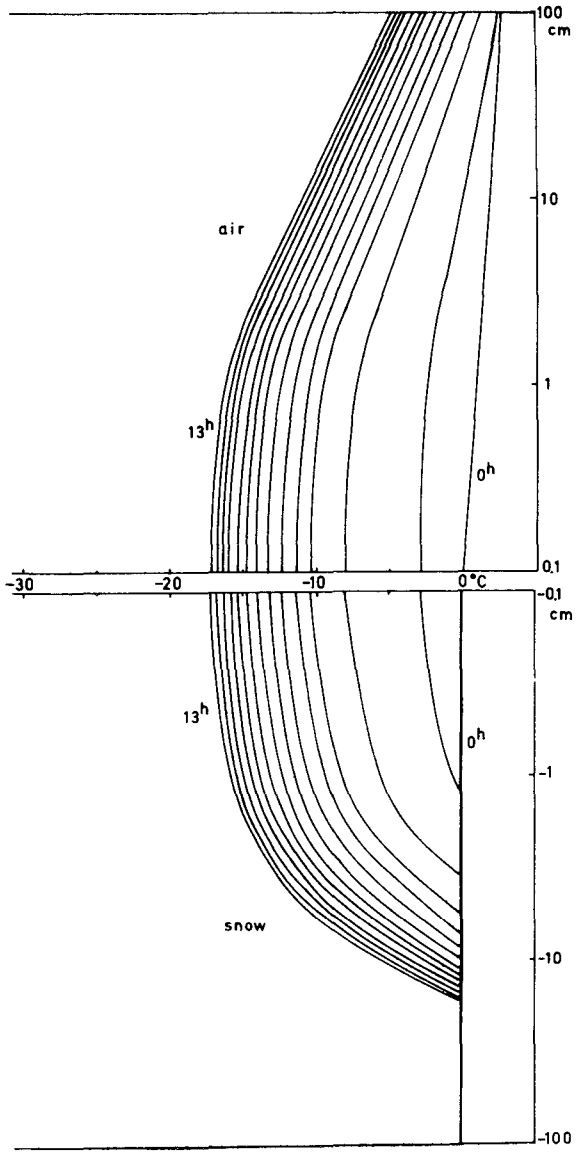

Fig. 23 Numerical variations of snow and air temperatures in snow-melting season.

snow-melting season: The reflectivity of snow for long-wave radiation $\alpha_L = 0$, the density of snow $\rho = 0.35$ g/cm^3, the density of air $\rho_a = 0.0013$ g/cm^3, the specific heat of air $C_{pa} = 0.24$ cal g^{-1}°C^{-1}, the heat conductivity of snow $\lambda = 8.0\times10^{-4}$ cal cm^{-1}°C^{-1}sec^{-1}, the specific heat of ice C_{pi}=0.5 cal g^{-1}°C^{-1}, the thickness of an air layer H=250m, and the depth of a snow cover D=1m. Such a large temperature difference as 10°C was obtained from these calculations between the height of 100cm and the snow surface, but actual observations showed that it was only 5°C. This disagreement may result from the calculations in which the radiative flux divergence is neglected in the air near the surface. The cooling rate was large for the first 3 to 4 hours, after which it became small. In the snow-melting season (Fig.23), there is no temperature gradient in the snow cover at the beginning, but a layer in which the temperature changes develops in the upper part of the snow cover, reaching to the depth of 14cm in 13 hours. This layer is called a crust layer.

Figure 24 shows the temperature profiles of a snow cover. It takes two hours from the beginning to bring about a temperature drop of about 10°C near the surface in winter,

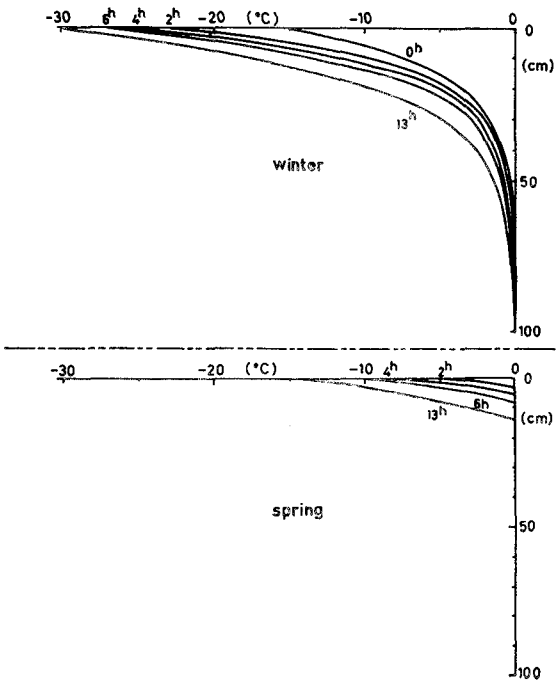

Fig. 24 Calculated temperature profiles of a snow cover.
Top : in winter, Bottom : in snow-melting season

but during the same hours a temperature drop of 5°C is brought about in the snow-melting season. Furthermore, the snow layer in which temperature change takes place is about 60 cm in thickness in winter and 14 cm in the snow-melting season.

(2) *Variations of surface temperature with time*

The surface temperature variation with time at night is calculated. First, it is assumed that this change occurs due only to a radiative heat loss which is represented by the equation

$$\Delta T=\frac{2}{\sqrt{\pi}}\frac{\sigma T_0^4-I_L\downarrow}{\sqrt{\rho C\lambda}}\sqrt{t} \tag{14}$$

The results of observations and calculations are plotted for comparison in Fig.25. Solid lines show observational values and broken lines calculated values. It shows a relatively good agreement as regards values for Jan.26 to 27, but as regards values for Jan.25 to 26 it does not. Neglect of sensible and conductive heat terms in eq.(14) causes calculated values to be smaller than observed values. Calculational results might be the lowest values considered. Secondly, eq.(1) is represented by the following, using the surface temperature T_0 :

$$(1-\alpha_S)I_S+(1-\alpha_L)(I_L-\sigma T_0{}^{i4})+\rho_a C_p K_1^i\frac{\theta_1^i-T_0^i}{\Delta Z_1}$$
$$+\lambda\frac{T_0^i-T_{-1}^i}{\Delta Z}=0 \tag{15}$$

and the value of T is obtained by solving this biquadratic equation with respect to T.

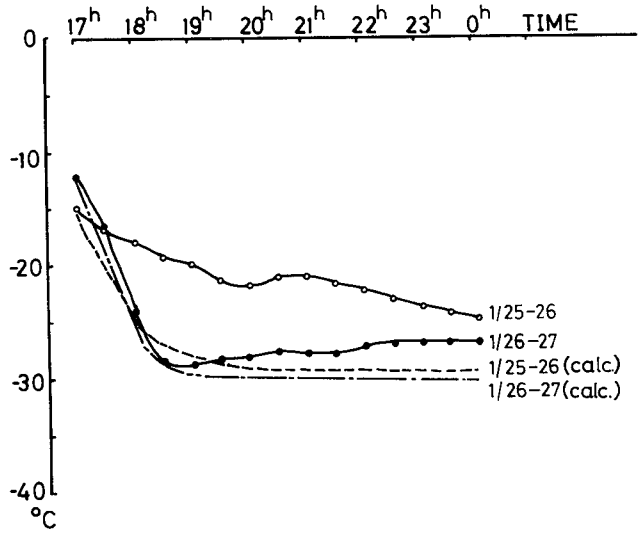

Fig. 25 Variation of snow surface temperature
Broken line : values calculated from Brunt's equation
Solid line : observational values

Solid and broken lines in Fig.26 show values by observation and calculation, respectively. They are in good agreement for both winter and the snow-melting season. These observational periods were favored by such good conditions like clear calm nights that they were represented by the simple model which was used in this calculation. Namely, it may be said that during a period in which radiative cooling takes place a surface temperature variation can be obtained by using the heat balance equation.

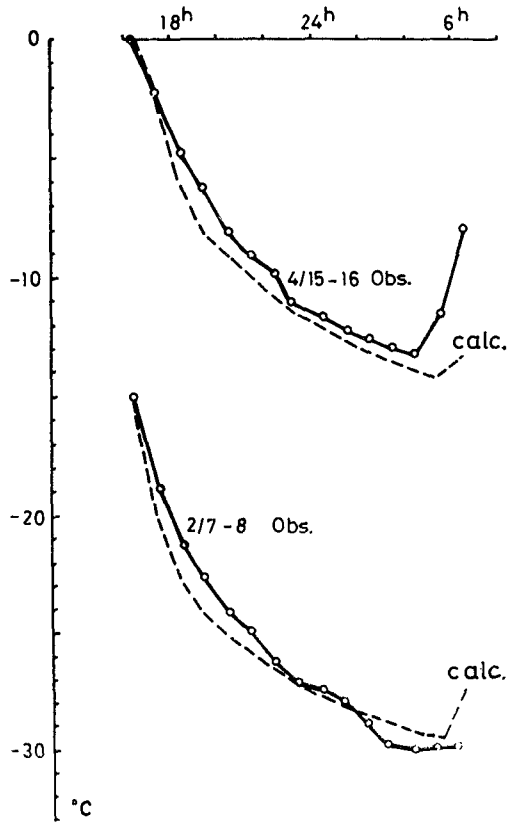

Fig. 26 Variations of snow surface temperature with time.
Broken line : values calculated from heat balance equation over the surface
Solid line : observational values

(3) *Progress of a refreezing (crust) layer in a snow cover*

The progress of a crust layer is estimated using eq.(10) and compared with measured values in Fig. 27. Calculated and measured values are shown by lines I and III, respectively. The calculated values are in good agreement with the measured values during the first five hours, but then the former values become smaller than the latter. This is explained by an assumption for the calculations that a liquid water content is kept constant all the time throughout the entire snow cover. However, in actuality a liquid water content is not uniformly distributed in the snow cover; that is, it decreases as the position lowers from the surface to the bottom of the snow cover (YOSHIDA 1962), and some portions of the liquid water move downward during the growth of a crust layer. Namely, if the amount of liquid water which exists near the snow surface is used in the calculations, such a value accounts for an overestimated one as compared with the actual one at some depth; therefore, the thickness of the crust layer obtained by the calculation

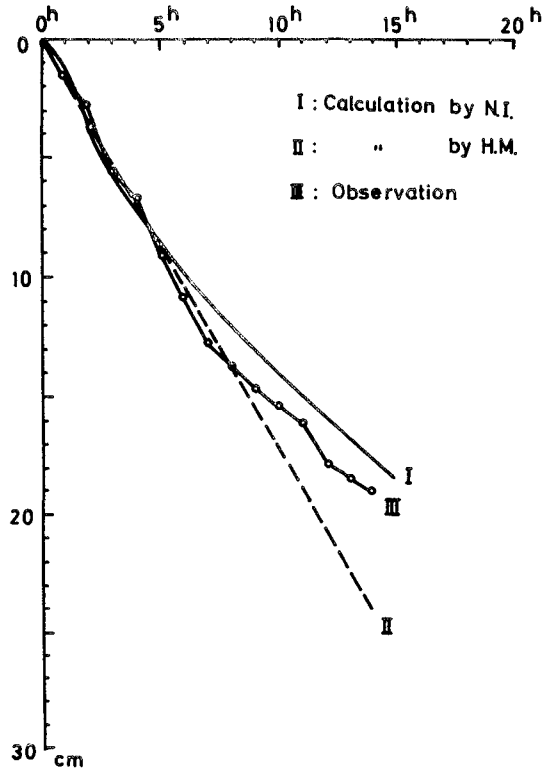

Fig. 27 Comparison between calculated (I) and measured (II) thicknesses of a crust layer.

becomes smaller. The results which are derived by using MATSUOKA'S equation (1968) are plotted on this figure, as shown by the broken line II. They are also in good agreement with the observational values during the first several hours, then the calculated values become larger conversely. This is explained by the fact that for his calculation the maximum amount of net radiation which is obtained about two hours after the beginning of refreezing is used and kept constant during the calculations, so a heat loss from the snow surface may be overestimated. Actually the amount of net radiation becomes smaller, approaching zero, as the surface temperature drops.

(4) *Heat balance in winter and the snow-melting season*

Using the values obtained from the calculations mentioned above, each component of the heat balance at the lower station was estimated for winter and the snow-melting season, respectively (in Fig. 28). Each value is represented by a percentage of the total heat amount. It is clearly shown that a heat loss from the surface is due only to a nocturnal radiation and that a supplied heat energy to the surface is due to a sensible heat flux. Some portions of the heat loss (about 20 %) due to radiation are compensated by the sensible heat flux for both seasons. The rest of this heat loss is about 80 %, which is balanced by the heat loss of the snow cover in winter. As for the snow-melting season a latent heat is released by a phase change, so the total heat loss from the snow cover is about 20 %. These results are in good agreement with observational results described in the previous chapter.

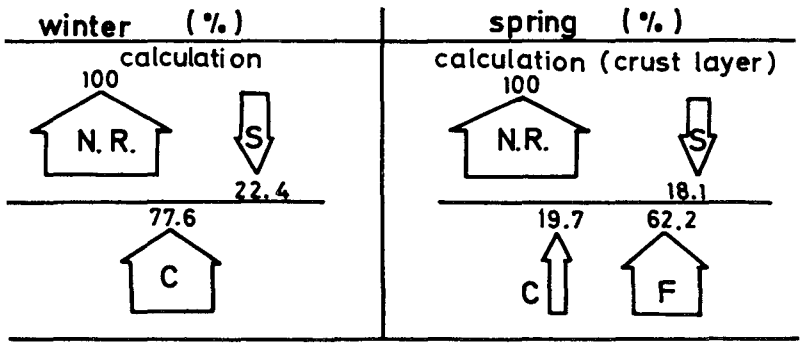

Fig. 28 Comparison of numerical heat balance components between winter and snow-melting season.

V. Consideration of air temperature and air flow at a land basin

V—1 *Variations of air temperature due to* radiative flux divergence

Variations of air temperature were estimated by numerical calculations, but the calculated values at 100 cm above the surface were different from the observed values as mentioned before. The radiative heating or cooling due respectively to radiative absorption or divergence in the air might be considered to be one of the reasons. The surface temperature is lower than the temperature at the higher level when a temperature inversion occurs. In such a case radiative cooling may occur in the air layer due to radiative flux divergence above the surface. The actual cooling rate should be represented by the following equation (FUNK 1960) :

$$\frac{\partial\theta}{\partial t} = \frac{1}{C_p\rho_a}\text{div } Q_N + \frac{1}{C_p\rho_a}\text{div } Q_T \qquad (16)$$

where div $Q_N = \frac{\partial Q_N}{\partial Z}$ is the radiative heat flux divergence and div $Q_T = \frac{\partial Q_T}{\partial Z}$ is the eddy heat flux divergence. Setting two net radiometers at two different heights above the surface, instantaneous measurements of net radiation were carried out. The two radio-

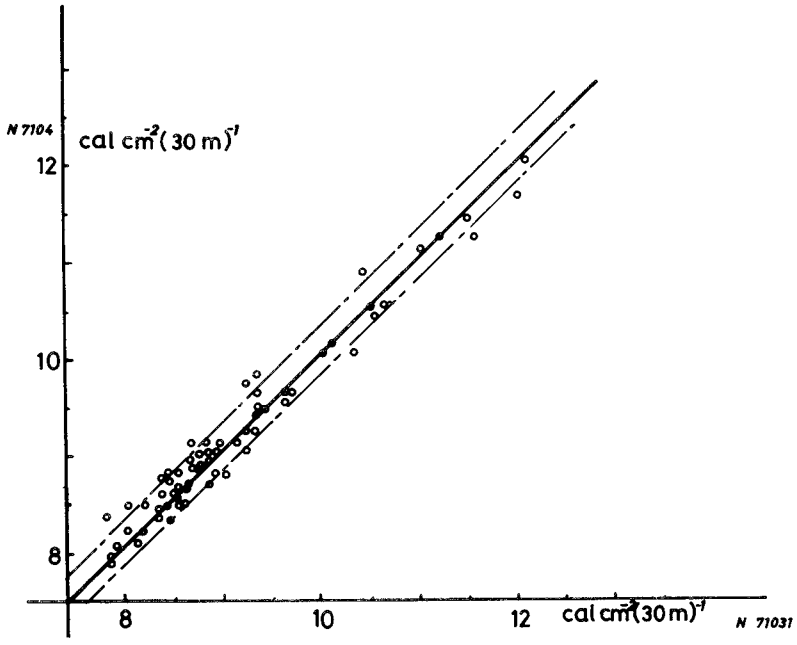

Fig. 29 Calibration lines for two net radiometers.

meters having their own characteristics, values obtained by them at the same height do not agree with each other precisely as shown in Fig. 29. Therefore, two radiometers were set at the same height for a long time before measuring the radiative flux divergence, and their readings were corrected by comparing with the values obtained by a standard instrument.

Figure 30 shows the actual and radiative cooling rates every 30 minutes. While the latter is always larger than the former, this difference might be due to divergence of an eddy heat flux as shown in eq.(16). In this case the maximum amount of radiative flux divergence in the air layer 130 cm in thickness was observed to be 1.5×10^{-3} cal cm^{-2} (30min)$^{-1}$ and the radiative cooling rate was calculated as -4.8°C/30min. Furthermore, a relation between the net radiation amount and actual cooling rate is shown in Fig. 31. The abscissa represents the net radiation amount Q_N (cal cm^{-2} hr^{-1}) and the ordinate the actual cooling rate ΔT(°C). The air temperature does not decrease as soon as the net radiation amount becomes negative, but it begins to decrease when the net radiation

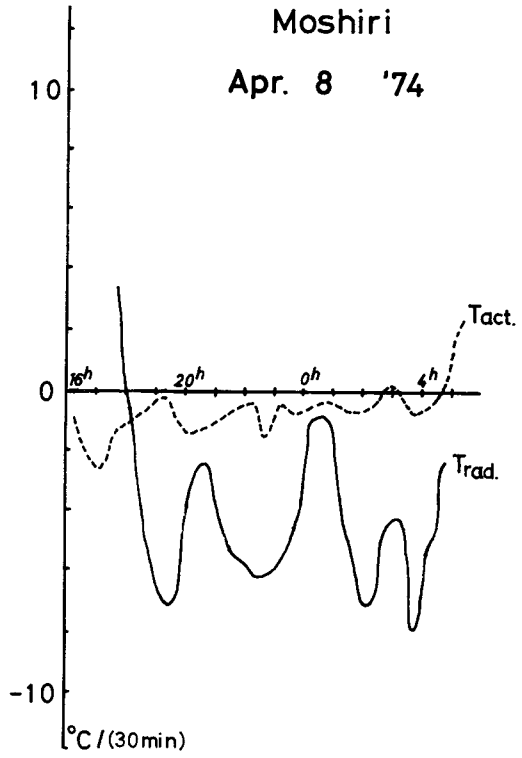

Fig. 30 Comparison between radiative and actual cooling rates.

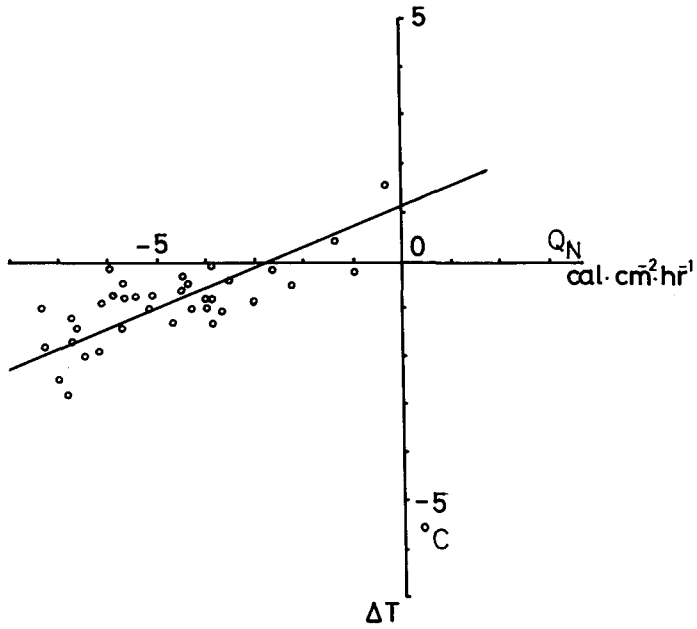

Fig. 31 Relation between net radiation amount and cooling rate.

amount becomes below -2 cal/cm^2. From this result, a heating effect due to divergence of an eddy heat flux is considered to exist. Though the order of this radiative cooling rate can be estimated, it is hard to obtain the accurate radiative flux divergence directly, because of its measuring accuracy. Recently another method has been tried; namely, at first, the cooling rate due to divergence of an eddy heat flux is measured using an ultra-sonic anemo-thermometer; next, its difference from the actual cooling rate is obtained; then, the difference is compared with the value derived from a radiative transfer theory. Not perfected yet, this method is being developed.

V — 2 *Variations of air temperature at a mountaintop in relation to a topographical feature*

Since a strong wind is usually blowing at a mountaintop which is located at a higher altitude, the sensible heat amount supplied to the surface of the mountaintop becomes large and the temperature near the mountaintop hardly drops. On the other hand, there is a chance in which wind speed becomes weak at the higher place: In this case there is the difference of cooling rate with time due to the topographical feature of the mountaintop. For example, at relatively narrow ridges existing in Moshiri and Toikanbetsu temperatures do not change very much even if a wind is relatively weak at the moun-

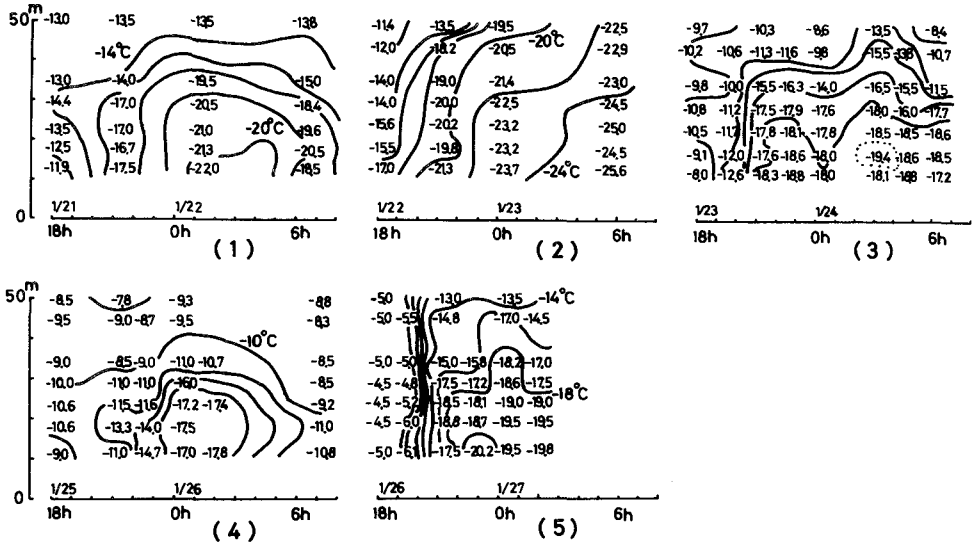

Fig. 32 Variations of isotherm with time along a mountain slope.
Interval of contour lines : 2°C

taintop, but in Tomakomai, whose feature is a plateau, the temperature measured at the higher place falls, whereby the strength of temperature inversion becomes small. Figure 32 shows the vertical temperature profiles along a hill slope. Usually as shown in (1),(3) and (4) in this figure, the temperature drops at the bottom site and it does not change very much at the top site, as a result of which an intense inversion develops. Meanwhile, as shown in (2) in this figure, when wind speed is low at the hill top, a very low temperature appears there and an inversion becomes weak. This is explained by the theory of temperature change of an advection flow. Figure 33 shows the cooling rates of an air flow blowing across one mountaintop 20 m in width and the other mountaintop 200 m in width shown by broken and solid lines, respectively. It is assumed that the boundary surface loses constantly as much heat as 3 cal per unit area during an interval of every 30 minutes and that a perfect heat exchange takes place between the boundary surface of the mountaintop and an air mass blowing over it. The abscissa represents the time after the air mass comes into contact with the boundary surface and the ordinate the cooling rate of the air mass, where a is the reciprocal number of its volume. Assuming an air mass of 10^3 cm^3 in volume moves with a wind speed of 1 m/s across the surface boundary of the mountaintop 200 m in width, it brings about a temperature change of 1°C in 200 sec when it leaves the mountaintop, but in case of the mountaintop 20 m in width the degree of its cooling is 0.1°C. It is shown that, if wind speed becomes smaller and the width of the surface boundary wider, the cooling progresses. Namely, the boundary

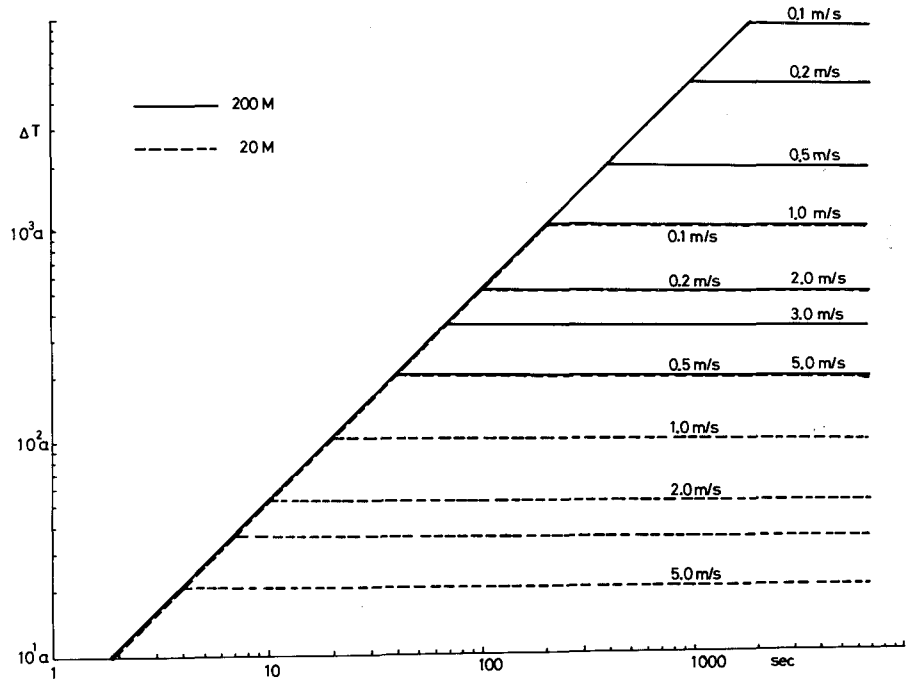

Fig. 33 Difference of cooling rates with wind speed and width of a boundary layer.

surface of a mountaintop acts as a cooling plane for the air mass which moves over the mountaintop. In other words, a narrow mountain ridge constitutes such a narrow cooling plane that, even if a wind is weak, the time during which an air mass passes over this plane is short, making it difficult to cool the air mass. But in the case of a plateau like terrain it takes such a long traverse time that an air mass passing is considerably cooled in the same way as the air mass moves over a flat and wide plain.

V—3 *Air flow on a mountain slope*

The type of air flow which is found in some reports about a cold air drainage on a mountain slope (BERGEN 1969, IMAOKA 1974), was subjected to observations on one of the slopes located in surrounding mountains of the Moshiri basin during the time when radiative cooling occurred. This site has a length of 500 m, a width of 50 m and a mean slope angle (inclination) of 5°. Wind speeds were measured at a height of 1 m above the surface at the highest and the lowest point of the slope and at a height of 25 cm at three other points in the intermediate parts of the slope. Besides, at one of the intermediate parts, wind speeds were measured at three different height, 25, 140 and 340 cm above the surface so that a wind profile was obtained. Figure 34 shows wind speed variations with time measured at one of the intermediate parts. Usually, the higher above the

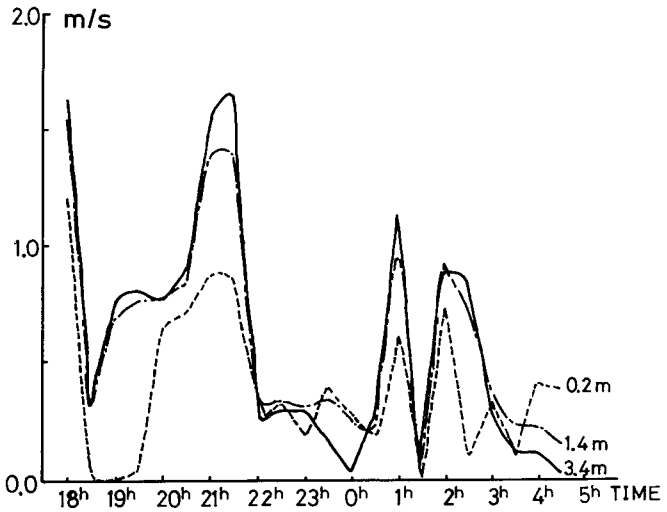

Fig. 34 Variations of wind speed with time at a mountain slope under inversion conditions.

snow surface, the larger becomes the wind speed, but a wind inversion was observed twice (2230 to 0030 and 0300 to 0430 hours). At the same time, wind speeds measured at the bottom of the basin were below 0.2 m/s, while they averaged 1.5 m/s at the highest part of the slope, their direction being upslope. The results of the same measurement made in Toikanbetsu are shown in Table 2. The mean air flow with a

Table 2 Velocity of down air flow under inversion conditions.

Height (cm)	0 – 5	10	20	50	100
Speed (cm/s)	60 – 70	80 – 90	30	20	10

speed of 1 m/s was blowing upslope at a height of 2.5 m above the surface, but there was a down air flow with the maximum speed of 80 to 90 cm/s near the surface. The temperature of this down air flow was about −13°C, which was not so low, but at the bottom of the basin it was about −25°C. Namely, it is likely that the down air flow does not bring a cold air mass to the lower part of the basin, but pile up above the stable cold air mass which had been already made over the bottom of the basin, whereby it increases the thickness of a cold air layer thus contributing to the growth of a cold air lake. On the other hand, if a mountain has a broad plateau-like top, a cold air mass created there moves down the slope at times, the typical examples of which were observed on Antarctic slopes (LETTAU 1966, STRETEN 1963). Such a down air flow was also observed by the author on a mountaineous glacier which was surrounded by high mountains at both sides (STRETEN and others 1974).

Ⅳ. Concluding remarks

The following are concluding remarks from observations of radiative cooling in land basins made in Hokkaido during snowy seasons:

1) Extremely low temperature were observed at the bottom of a basin under the conditions of calm wind during a clear night.
2) Such extremely low temperatures were not brought from surrounding mountain slopes, but were made by local cooling at the bottom of the basin.
3) Usually air temperature hardly decreased at a mountaintop not so high, but it decreased very much at the bottom of the basin; consequently, a large temperature difference occurred between the two places. Furthermore, the inversion strength was weaker in the snow-melting season than in winter.
4) These results was explained by heat balances at the mountaintop and the bottom both in winter and the snow-melting season. Namely, at the bottom of the basin the amounts of sensible and latent heat transfers were so small that they cannot compensate for a heat loss due to negative net radiation; therefore, the temperature near the surface falls. On the other hand, at the mountaintop the air temperature hardly decreased as a result of an existence of a large sensible heat flux and an advective effect. Moreover, in the snow-melting season an important role was played in a heat balance by the latent heat which originated from refreezing of meltwater in a snow cover.
5) An estimation was made possible of a temperature variation with time (or cooling rate) near the snow cover at the time of radiative cooling by solving a heat balance equation at the surface.

Acknowledgements

The author is grateful to the staff of the Moshiri and Teshio Experimental Forests of Hokkaido University and the members of snow avalanche and frost heaving sections of the Institute of Low Temperature Science (I. L. T. S.), Hokkaido University, for their logistic support, and Dr. M. Sekine and other researchers of the Radiative Center, Observation Division of the Japan Meteorological Agency for the calibration of the radiometers used. The author also would like to express his sincere gratitude to the members of snowmelt and meteorological sections of I. L. T. S. for the collection of numerous field data, and Dr.C.Magono of Hokkaido University and Dr.G. Wendler of University of Alaska for their useful comments on this investigation, and Dr.T.Ishida and Dr.K.Kojima of I.L.T.S. for every encouragement and valuable advice accorded in preparation for this paper.

Reference

BERGEN, J. D. 1969 Cold air drainage on a forested mountain slope. *J. Appl. Meteorol.* **10**, 684-693.

CARSLOW, H. S. and JAEGER, J. C. 1959 Conduction of heat in solids. Oxford University Press, 510pp.

de La CASINIÈRE, A. C. 1974 Heat exchange over a melting snow surface. *J. Glaciol.* **13**, 55-72.

FUNK, J. P. 1960 Measured radiative flux divergence near the ground at night. *Quart. J. Roy. Meteorol. Soc.*, **86**, 382-389.

GEIGER, R. 1965, The Climate near the Ground. Harvard University Press, Cambridge, Massachusetts, 661pp.

IDSO, S. B. and COOLEY, K. R. 1971 The vertical location at net radiometers I. The effects of underlying air layer. *J. Meteorol. Soc. Japan,* Ser.II, **49**, 343-349.

IMAOKA, E. 1974 Observations and considerations on the structure of the down slope wind. *J. Agricultural Meteorol.* **20**, 17-23.

KOJIMA, K., KOBAYASHI, D., ABURAKAWA, H., NARUSE, R., ISHIMOTO, K., ISHIKAWA, N. and TAKAHASHI, S. 1971 Studies of snow melt, runoff and heat balance in a small drainage area in Moshiri, Hokkaido. II. *Low Temp. Sci.* **A 29** 159-176.

KONDO, J. 1967 Analysis of solar radiation and downward long wave radiation data in Japan. *Sci. Rep. Tohoku Univ.* Ser., 5, **18**, 91-124.

KONDO, J. 1972 Difference between the net radiation at the ground surface and that measured at the height of net radiometer. *J. Meteorol. Soc. Japan,* Ser. II. **50**, 381-383.

LACHAPELLE, E. R. 1959 Annual mass and energy exchange on the Blue Glacier. *J. Geophy. Res.* **64**, 443-449.

LETTAU, H. 1949 Isotropic and non-isotropic turbulence in the atmospheric surface layer. Geophysical Research Paper, U. S. AFCPL, No.1, Cambridge, 86pp.

LETTAU,H. H. 1962, Theoretical wind spirals in the boundary layer of a barotropic atmosphere. *Beit. Phy. Atmos.* **35**, 195-212.

LETTAU, H. H. 1966, A case study of katabatic flow on the south polar plateau. *Antarctic Res. Ser.* 9, American Geophysical Union, washington, D. C., 1-11.

MATSUOKA, H., SHIMIZU, T. and ITO, F. 1968 Some considerations about examples of observations on diurnal variation of melting of snow cover and properties of deposited snow (1). *Mem. Fac. Edu. Fukui Univ.,* Ser. II, Nat. Sci., No.18, Part 1, 1-22.

MAYKAT, G. A. and UNTERSTEINER, N. 1969 Numerical prediction of the thermodynamic response of arctic sea ice to enviromental changes. The Rand Corporation, Santa Monica, California, RM-6093-PR, Nov. 172pp.

MUNN, R. E. 1966 Descriptive Micrometeorology. Academic Press, 242pp.

STRETEN, N. A. 1963 Some observations of Antarctic katabatic winds. *Australian Meteorol. Magazine,* **42**, 1-23.

STRETEN, N. A., ISHIKAWA, N. and WENDLER, G. 1974 Some observations of the local wind regime on an Alaskan Arctic Glacier. *Arch. Met. Geoph. Biokl.*, Ser. B, **22**, 337-350.

WELLER,G. E. 1968 The heat budget and heat transfer processes in Antarctic plateau ice and sea ice. Anare Scientific Reports, Series A (IV), Glaciology, No.102, 155pp.

WENDLER, G. 1971 As estimate of the heat balance of a valley and hill station in Central Alaska. *J. Appl. Meteorol.* **10**, No.4, 684-693.

WENDLER, G. and JAYAWEERA, K. O. L. F. 1972 Some measurements of the development of the surface inversion in Central Alaska during winter. *Pure and Appl. Geophys.*, **99**, 209-221.

WENDLER, G. and ISHIKAWA, N. 1973 Heat balance investigation in an arctic mountaineous area in Northern Alaska. *J. Appl. Meteorol.*, **12**, No.6, 955-962.

WENDLER, G. and ISHIKAWA, N. 1973 Experimental study of the amount of ice melt using three different methods. *J. Glaciol.*, **12**, 399-410.

WENDLER, G. and WELLER, G. 1974 A heat balance study of McCall Glacier, Brooks Range, Alaska. *J. Glaciol.*, **13**, 13-26.

YAMAMOTO, G. and SHIMANUKI, A. 1966 Turbulent transfer in diabatic condition. *J. Meteorol. Soc. Japan.* **44**, 301-307.

YOSHIDA, Z. and IWAI, Y. 1947 Measurement of thermal conductivity of a mass of snow. *Low Temp. Sci.* **3**, 79-87.

YOSHIDA, Z. 1962 Distribution of melt water within a snow cover. *Low Temp. Sci.*, **A 20**, 181-185.

YOSHINO, M. 1975 Climate in a small area. University of Tokyo Press, 549pp.

YOSHINO, M. 1971 Microclimate. Chijin syokan, 274pp.

ZDANKOWSKY, W. G. 1966 The nocturnal temperature minimum above the ground. *Beit. Phys. Atmos.*, **39**, S. 247-253.